ACS APPLIED NANO MATERIALS

Open Access

This article is licensed under CC-BY 4.0

www.acsanm.org

Article

CdSe Quantum Dot-Based Delivery System for CRISPR-Cas9 Mediated Microglial Gene Modulation

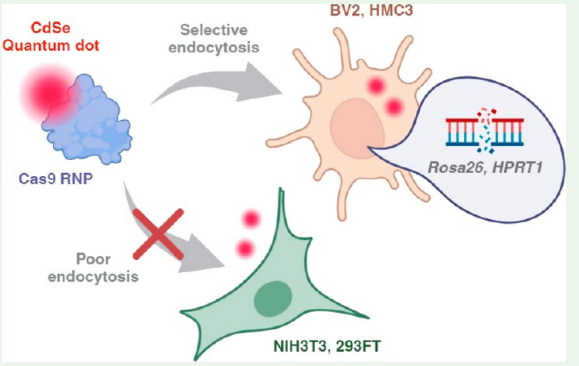
Hyeon-Gu Yeo,[○] Jinyoung Won,[○] Lee Wha Gwon,[○] Seokbeom Roh, Wi-Jae Lee, Kyung Seob Lim, Chang-Yeop Jeon, Junghyung Park, A Reum Je, Jincheol Seo, Jiyeon Cho, Jung Bae Seong, Yu Gyeong Kim, Keonwoo Kim, Sangwoo Lee, Sung-hyun Park, Won Seok Choi, Yang Hoon Huh, Gyudo Lee, Hyoung-Chin Kim, Seung Hwan Lee,* and Youngjeon Lee*

Cite This: *ACS Appl. Nano Mater.* 2024, 7, 24013−24027

Read Online

ACCESS | Metrics & More | Article Recommendations | Supporting Information

ABSTRACT: Microglia, the primary immune cells of the central nervous system, play a crucial role in neuroinflammation and homeostasis. They can adopt either M1 or M2 phenotypes, influencing their inflammatory and reparative functions. Modulating microglia phenotypes and functions is a significant area of therapeutic interest. However, the availability of delivery vehicles and gene expression modulation techniques targeting microglia is limited. Fluorescent quantum dots (Qdots) are semiconductor nanoparticles, specifically used to label and modulate microglia functions and offer promising alternatives to traditional genome editing methods. In this study, we developed a cadmium selenide (CdSe) Qdot-mediated delivery system to target the microglial genome. We evaluated streptavidin-coated CdSe Qdots for their ability to deliver clustered regularly interspaced short palindromic repeats-Cas9 to microglia in vivo and in vitro and assessed their distribution, safety, and capacity to deliver Cas9 ribonucleoproteins (RNPs) for gene editing by injecting the Qdots into the frontal white matter of cynomolgus monkeys and Sprague−Dawley rats. Assessing the mechanisms of Qdot uptake and stability revealed that CdSe Qdots were selectively taken up by microglia, with minimal localization in other cell types. Histological and biochemical analyses revealed no significant inflammatory or toxic effects following Qdot injection. The Qdots did not interfere with Cas9 RNP gene editing efficiency and provided enhanced fluorescence signals in microglia. Cas9/Qdot conjugates were stable and effectively delivered CRISPR-Cas9 to microglia, demonstrating higher specificity and lower cytotoxicity when compared to commercial delivery reagents. In conclusion, Qdots offer a promising nonviral method for targeted genome editing in microglia, indicating potential therapeutic applications for neuroinflammatory and neurodegenerative diseases. However, further optimization is needed to improve gene editing efficiency and safety for clinical applications.



KEYWORDS: *microglia, quantum dots, nonhuman primates, CRISPR-Cas9, ribonucleoprotein*

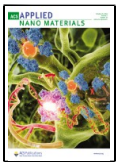
Downloaded via CHUNG-ANG UNIV on December 5, 2024 at 06:26:29 (UTC).
See https://pubs.acs.org/sharingguidelines for options on how to legitimately share published articles.

1. INTRODUCTION

Microglia constitute the primary immune cells of the central nervous system[1] and play a crucial role in neuroinflammation and homeostasis. Microglia become activated upon recognition of the pathogen-associated or damage-associated molecular patterns by toll-like receptors,[2] and undergo phenotypic changes. Activated microglia can adopt an M1 phenotype, characterized by their ability to phagocytose, present antigens, and produce pro-inflammatory cytokines such as tumor necrosis factor-alpha (TNF-α), interleukin-1 beta (IL-1β), IL-6, IL-12, IL-23, and interferon-gamma (IFN-γ).[3,4] Conversely, they can adopt an M2 phenotype, which is associated with tissue repair and the secretion of anti-inflammatory cytokines, such as transforming growth factor-beta (TGF-β), IL-10, IL-4, IL-13, IL-25, and growth factors including brain-derived neurotrophic factor (BDNF), epidermal growth factor, and insulin-like growth factor-1 (IGF-1).[4,5]

Microglia exert both detrimental and beneficial effects in neurodegenerative diseases.[3] Therefore, modulating their phenotypes and functions is an area of significant therapeutic interest. Current strategies for microglia modulation involve the use of IL-loaded lentivirus,[6] nanoparticle-mediated RNAi,[7] lentiviral RNAi systems,[8,9] gene delivery through adeno-associated virus (AAV),[10] clustered regularly interspaced

Received: August 9, 2024
Revised: September 17, 2024
Accepted: September 20, 2024
Published: October 8, 2024



© 2024 The Authors. Published by American Chemical Society

short palindromic repeats CRISPR-Cas9 mediated gene editing,[11,12] and organic chemicals, such as glucocorticoid and norepinephrine treatments.[13]

CRISPR-Cas9 system, a prokaryotic adaptive immune response, has emerged as a third-generation editing tool for targeted genome editing in various species and diseases.[14,15] Although cerebral genome editing is primarily performed using viral delivery methods, such as lentivirus[16] and AAV,[10,17] they pose several challenges owing to their immunogenicity and genomic damage caused by the random incorporation of exogenous genes.[18] Therefore, nonviral vectors, such as gold nanoparticles,[18] cationic lipid-assisted nanoparticles,[15] and modified 1,2-dioleoyl-3-trimethylammonium-propane-loaded lipid nanoparticles,[16] are being explored as safer alternatives for delivering CRISPR-Cas9 systems to brain cells.

Quantum dots (Qdots) are semiconductor fluorescent nanoparticles with a size of 2−10 nm, comprising a heavy metal core made of CdSe, cadmium telluride, or indium arsenide, and a passivating coating or shell.[19,20] These nanoparticles are highly valued in biomedical research owing to their beneficial effects, such as higher brightness than organic dyes, resistance to photobleaching, symmetry and narrowness of emission line widths with various color probes (525−800 nm), and surface availability for manipulation.[20,21] However, several unanswered questions should be addressed before the Qdots enter the clinical research phase. It is essential to comprehend how nonhuman primates react to Qdots for safe clinical applications. Nevertheless, only a few toxicological investigations[22,23] on heavy metal-based Qdots in nonhuman primates have been reported. To the best of our knowledge, no research on intracranial injection has been conducted. Moreover, because their side effects constitute a highly controversial topic, we analyzed the possibility of adverse effects after Qdot administration in vitro and in vivo.

Several methods have been developed for the surface functionalization of Qdots to improve their biocompatibility by aqueous solubilization using polyethylene glycol (PEG),[24] endolysosomal escape using polyethylenimine (PEI),[24,25] and conjugation with various materials, such as cytotoxic saporin,[19] paramagnetic gadolinium,[26] CRISPR ribonucleoproteins (RNPs),[27] and plasmid DNA.[24] Furthermore, Qdots can regulate microglia function owing to their microglia-specific endocytosis and labeling,[19,28] thereby making them promising candidates for microglia-specific applications.

However, little is known about the ability of microglia-targeted Qdot delivery to edit the genome; therefore, in this study, we introduce a novel strategy for microglia-targeted modulation by delivering CRISPR-Cas9 using Qdots and evaluate the efficacy and potential of this therapeutic strategy. We aimed to evaluate the selective uptake of streptavidin-coated CdSe Qdots by microglia. Additionally, we evaluated the molecular structure, cellular distribution, and the possibility of adverse effects of biotinylated Cas9 RNPs delivered via Qdots. We also determined the gene knockout efficiency of these engineered Qdots in targeting key genomic safe harbors, such as the mouse *Rosa26* and human *HPRT1* loci. Consequently, these studies will enhance the understanding of the distribution, intracellular fate, microglia-targeted genome editing, and possibility of adverse effects after Cas9/Qdot conjugate treatment.

2. EXPERIMENTAL SECTION

2.1. Experimental Animals and Ethical Statements. Three Sprague−Dawley (SD) rats (Koatech, Pyeongtaek, Korea) weighing 250−260 g were used in the pilot study. The rats were maintained on a 12:12 h light−dark cycle and allowed ad libitum access to commercial rodent chow (Cargill Agri Purina Inc., Sungnam, Korea) and water. Three female cynomolgus monkeys (*Macaca fascicularis*) aged 10−15 years, weighing 4−5 kg, were selected [Subacute stages post Qdot injection (N = 2) with a needle-injected control (stab wound injury model)] to study the biodistribution and safety assessment of injected Qdots. Subacute stages were defined based on a study by England et al.[29] The monkeys were imported from Suzhou Xishan ZhongKe Laboratory Animal Co., Ltd. (Suzhou, China) and Shin Nippon Biomedical Laboratories (Zhaoqing, China). They were housed in indoor cages at the National Primate Research Center of the Korea Research Institute of Bioscience and Biotechnology (KRIBB, Cheongju, Korea) and provided with commercial monkey chow (Envigo, Indianapolis, IN, USA), along with a daily addition of different fruits and *ad libitum* access to water. Their environment was carefully regulated, with a temperature of 24 ± 2 °C, a humidity level of 50 ± 5%, and a 12:12 h light−dark cycle. Testing for B virus, simian immunodeficiency virus, simian T-cell lymphotropic virus, and simian retrovirus infections was part of the routine management and monitoring of animal health. The Institutional Animal Care and Use Committee of the Korea Research Institute of Bioscience and Biotechnology (approval no. KRIBB-AEC-20269) approved all ethical procedures, which adhered to the guidelines of Animal Research Reporting of In Vivo Experiments and National Institutes of Health standards for the US.[30]

2.2. Surgical Procedures. We injected CdSe Qdots (Qdot Streptavidin Conjugates, Invitrogen, Carlsbad, CA, USA) into the frontal white matter of two cynomolgus monkeys and three SD rats. SD rats were anesthetized by intraperitoneal injection of ketamine (100 mg/kg) and xylazine (5 mg/kg). During surgery, the rats were placed on a stereotaxic frame (Neurostar, Tübingen, Germany) and fixed using ear bars (David Kopf, Tujunga, CA, USA). The Qdot solution (5 μL, 100 nM, and 0.4 μL/min) was stereotaxically administrated into the brain, at the following coordinates relative to bregma: anterior-posterior: 0, medial-lateral: ±3, and dorsal-ventral: −6. The skin wound was closed by suturing and treated with an antiseptic ointment (10% povidone-iodine). An antibiotic (enrofloxacin) and analgesic (ketoprofen) were administered (5 mg/kg, intramuscularly; IM) after surgery. The brains were perfused under anesthesia [ketamine (100 mg/kg) and xylazine (5 mg/kg) through intraperitoneal injection] and fixed 1 week after surgery.

The monkeys were fixed in a sphinx position using computed tomography and magnetic resonance imaging MRI-compatible stereotaxic frame, and a cocktail of ketamine (5 mg/kg, IM) and atropine (0.02 mg/kg) was used to induce anesthesia. Additional anesthesia was maintained using isoflurane (1.5% in 2 L/min oxygen). Once the head-restrained animal was confirmed to be inside the stereotaxic frame (Neurostar), a preoperative MRI was performed to obtain a baseline reference to target the brain region. The frontal white matter, the targeted brain region, was identified using stereotaxic coordinates of the baseline images. An MRI fiducial marker was used as a precise reference point. A burr hole, approximately 5 mm in diameter, was created using a medical drill. The Qdot solution (10 μL, 1000 nM) was injected into the frontal white matter via convection-enhanced delivery using a Hamilton syringe (Hamilton, Franklin, MA, USA) and a microinfusion pump (Neurostar). The initial infusion rate of the fluid was 0.2 μL/min. The rate was gradually increased to 0.4, 0.6, and 0.8 μL/min at intervals of 5 min. To confirm the accuracy of the injection location, a 1 μL gadolinium-based MRI contrast agent (5 mM) was coinfused with the Qdot solution. Following infusion, the syringe needle was gently removed from the brain after being in the intended area for 5 min. Throughout all surgical procedures, vital indicators, such as body temperature, pulse, oxygen saturation, and heart rate, were tracked while under anesthesia. The skin wound was closed by suturing and

https://doi.org/10.1021/acsanm.4c04586
ACS Appl. Nano Mater. 2024, 7, 24013−24027

treated with an antiseptic ointment (10% povidone-iodine) in the same manner as the surgical procedures in rats. An antibiotic (enrofloxacin) and analgesic (ketoprofen) were administered (5 mg/kg, intramuscularly) after surgery.

2.3. MRI. Ketamine (0.5 mg/kg, IM) was initially used to anesthetize monkeys. The monkeys were maintained with 1.5% isoflurane in 99.9% oxygen (2 L/min) for brain MRIs, placed in a customized stereotaxic frame, and immobilized in the sphinx position. The animal was kept warm by placing a blanket around it, and other vital signs, such as pulse, respiration rate, body temperature, inhaled CO_2 level, and O_2 saturation, were continuously monitored. MRI experiments were conducted using a 3.0 *t* MRI scanner (Achieva 3.0T; Philips Medical Systems, Best, Netherlands) with a 32-channel head coil. Three-dimensional sagittal T1-weighted images were acquired using a Turbo Field Echo sequence with a TR/TE of 14/6.9 ms, 150 × 150 field-of-view, matrix size 300 × 300, 1.0 mm slice thickness, −0.5 mm slice gap, flip angle 8°, acquisition voxel size 0.5 × 0.5 × 1.0, 75 slices and an average of 4.

2.4. Hematological and Biochemical Analyses. Blood samples were collected from the femoral veins of the monkeys for safety assessment of the administered Qdots. Blood tests were conducted for hematological and biochemical investigations using a HEMAVET 950FS (Drew Scientific, Cumbria, UK) and Dri-Chem 7000i (Fujifilm, Tokyo, Japan), respectively. Reference values for cynomolgus monkeys were obtained from a previous study.[31]

2.5. Slice Preparation and Immunohistochemistry. We acquired the brains of cynomolgus monkeys 1 ($N = 1$) and 2 weeks ($N = 1$) after Qdot injection with a control. Under isoflurane-induced anesthesia (1.5% in 2 L/min oxygen), the brains were perfused with cold phosphate-buffered saline (PBS), postfixed in 4% paraformaldehyde (PFA) for 24 h at 4 °C, and then cut into 4 mm coronal slices using a customized monkey brain slicer. The brain slices were submerged in PBS containing 30% sucrose. Following tissue dehydration, the brain slices were embedded in a compound at an appropriate cutting temperature and then frozen at −80 °C. The embedding blocks were cut on a cryostat into 30 μm thick sections, blocked for 1 h with 5% normal goat serum by free-floating and incubated for 12 h at 4 °C with the following primary antibodies: polyclonal rabbit ionized calcium-binding adapter molecule 1 (IBA1; GeneTex, Irvine, CA, USA), monoclonal rabbit neuronal nucle (Abcam, Cambridge, UK), polyclonal rabbit glial fibrillary acidic protein (GFAP; Abcam), polyclonal rabbit IL-6 (GeneTex), polyclonal rabbit TNF-α (GeneTex), polyclonal rabbit IL-10 (GeneTex), and polyclonal rabbit TGF-β (GeneTex). For immunofluorescence, the sections were incubated at room temperature with Alexa Fluor 488 goat antirabbit secondary antibody (Abcam) in the dark for 1 h. Additionally, a terminal deoxynucleotidyl transferase dUTP nick end labeling (TUNEL; Roche Applied Science, Basel, Switzerland) assay was performed and incubated for 1 h at 37 °C, following the manufacturer's instructions. Subsequently, the sections were mounted with 4′,6-diamidino-2-phenylindole (DAPI) VECTASHIELD antifade mounting medium (Vector Laboratories, Burlingame, CA, USA) for nuclei counterstaining, and images were acquired using a fluorescence microscope (BX51, Olympus, Tokyo, Japan), a confocal microscope (LSM 700, Carl Zeiss Meditec, Dublin, CA, USA), and a fluorescence-labeled organism bioimaging instrument (FOBI, Cell Gentek, Daejeon, Korea). Qdot-labeled microglial cells were quantified in two areas (injection and peri-injection cores) using the ImageJ software (National Institute of Health, Bethesda, MD, USA). We determined the peri-injection core at a site 2 mm from the injection point.

2.6. Quantification of Qdot Treatment with Lipopolysaccharide in BV2 Cells. To identify the cytotoxicity of the Qdots, we treated BV2 (7×10^4 cells/mL) cells with 1 and 5 nM Qdots. To determine whether Qdots interfered with inflammatory cytokine production through LPS (0.5 μg/mL; from *Escherichia coli* O111:B4; Sigma-Aldrich, St. Louis, MO, USA) stimulation in the following 48 h, we performed pretreatment (Qdot → LPS) or cotreatment (Qdot + LPS) with Qdots. After treatment, the samples were quantified using an ImageJ cell counter (National Institutes of Health) and a nitric oxide (NO) detection kit (iNtRON Biotechnology, Seoul, Korea), and cell viability was determined using a Cell Counting Kit-8 (Dojindo Laboratories, Kumamoto, Japan), following the manufacturer's instructions. Additionally, cell supernatants were collected by centrifugation (1000 ×*g* for 10 min at 4 °C) and stored at −80 °C. The samples (75 μL) were evaluated using mouse multiplex assay kits (monocyte chemoattractant protein-1 [MCP-1], TNF-α, IL-6, IL-1β, IL-23, TGF-β1, IL-10, IGF-1, BDNF, IL-4, IL-13, and IL-25) (R&D Systems, Minneapolis, MN, USA). Assays (Koma Biotech, Seoul, Korea) were performed in triplicate, and the median fluorescence intensity corresponding to each cytokine was measured using a magnetic Luminex (Austin, TX, USA).

2.7. Purification of Recombinant SpCas9. Purification of recombinant SpCas9 was performed following the protocols described by Globyte et al.[14] and Kim et al.[32] In *E. coli* BL21 (DE3, Rosetta), the pET plasmid encoding (6 ×) his-tagged SpCas9 was introduced. The Cys80 residue of SpCas9 was mutated to serine (C80S) using SnapGene design (GSL Biotech, Chicago, IL, USA) for additional investigation. The transformed bacteria were transferred to 250 mL LB medium containing 50 μg/mL kanamycin. The culture was incubated for 24 h at 18 °C with shaking (180 rpm). Next, 0.5 mM isopropyl β-D-1-thiogalactopyranoside was inoculated at 18 °C for 48 h, followed by harvesting the cells via centrifugation (5000 ×*g*) for 10 min (at 4 °C). The cell pellet was resuspended with lysis buffer (20 mM Tris-HCl (pH 8.0), 300 mM NaCl, 10 mM β-mercaptoethanol, 1% Triton X-100, and 1 mM phenylmethylsulfonyl fluoride; Sigma-Aldrich) and sonicated on ice. Thereafter, the lysate was centrifuged at 5000 ×*g* for 10 min (4 °C), and the supernatant was mixed with 2 mL nickel-nitrilotriacetic acid (Ni-NTA) slurry (QIAGEN, Valencia, CA, USA) at 4 °C for 90 min. The mixture was then washed multiple times with a premade wash buffer (20 mM Tris-HCl [pH 8.0] and 500 mM NaCl), and the (6 ×) His-tagged SpCas9 was eluted with elution buffer (20 mM Tris-HCl [pH 8.0], 300 mM NaCl, and 200 mM imidazole) to remove nonspecific binding components. Finally, the buffer containing eluted SpCas9 protein was modified for storage (10 mM HEPES-KOH [pH 7.5], 250 mM KCl, 1 mM MgCl2, 0.1 mM EDTA, 7 mM β-mercaptoethanol, and 20% glycerol) using a centrifugal filter (Amicon Ultra 100 K, Danvers, MA, USA). The purified SpCas9 protein was frozen in liquid nitrogen and stored at −80 °C.

2.8. Qdot Conjugation with Cas9. Thiol-maleimide and biotin−streptavidin interactions were used to conjugate Cas9 to Qdots. Briefly, disulfide bonds of purified Cas9 were reduced using 10 mM tris (2-carboxyethyl) phosphine hydrochloride (TCEP-HCl; Thermo Scientific, Sunnyvale, CA, USA) at room temperature for 30 min. After reduction, TCEP was appropriately removed using a centrifugal filter (Amicon Ultra 100 K). Next, a 20-fold molar excess of maleimide-PEG2-biotin (Thermo Scientific) was added to purified Cas9 in BupH Tris Buffered Saline (Thermo Scientific) and incubated overnight at 4 °C, with gentle mixing in a rotator. To remove the unbound maleimide-biotin chemicals, the mixed sample was washed using the Amicon Ultra 100 K centrifugal filter. Thereafter, a 10-fold molar excess of biotinylated Cas9 was conjugated to the Qdots at room temperature with continuous shaking for at least 3 h. Using the histidine−zinc interaction method, purified Cas9 and Qdots were conjugated in 10 mM sodium tetraborate buffer (pH 9.0, Sigma-Aldrich) at room temperature for 1 h. Imidazole buffer (20 mM Tris-HCl [pH 8.0], 300 mM NaCl, and 200 mM imidazole) was used to disrupt the histidine-zinc connection. Unconjugated Cas9 and Qdots were removed using a centrifugal filter (Vivaspin 300 K, Sartorius, Göttingen, Germany). Sodium dodecyl sulfate-polyacrylamide gel electrophoresis (SDS-PAGE), MultiMode 8 atomic force microscopy (AFM; Bruker Nano Inc., Santa Barbara, CA, USA), 4′-hydroxyazobenzene-2-carboxylic acid (HABA) biotin assay (Thermo Scientific), and 1% agarose gel electrophoresis were used to verify the protein-Qdot conjugation.

2.9. Atomic Force Microscopy and Transmission Electron Microscopy Analysis. AFM analysis was conducted under ambient conditions using a MultiMode 8 atomic force microscope (Bruker Nano Inc.) equipped with PR-T300 AFM tips (Probes Inc., Seoul,

https://doi.org/10.1021/acsanm.4c04586
ACS Appl. Nano Mater. 2024, 7, 24013−24027

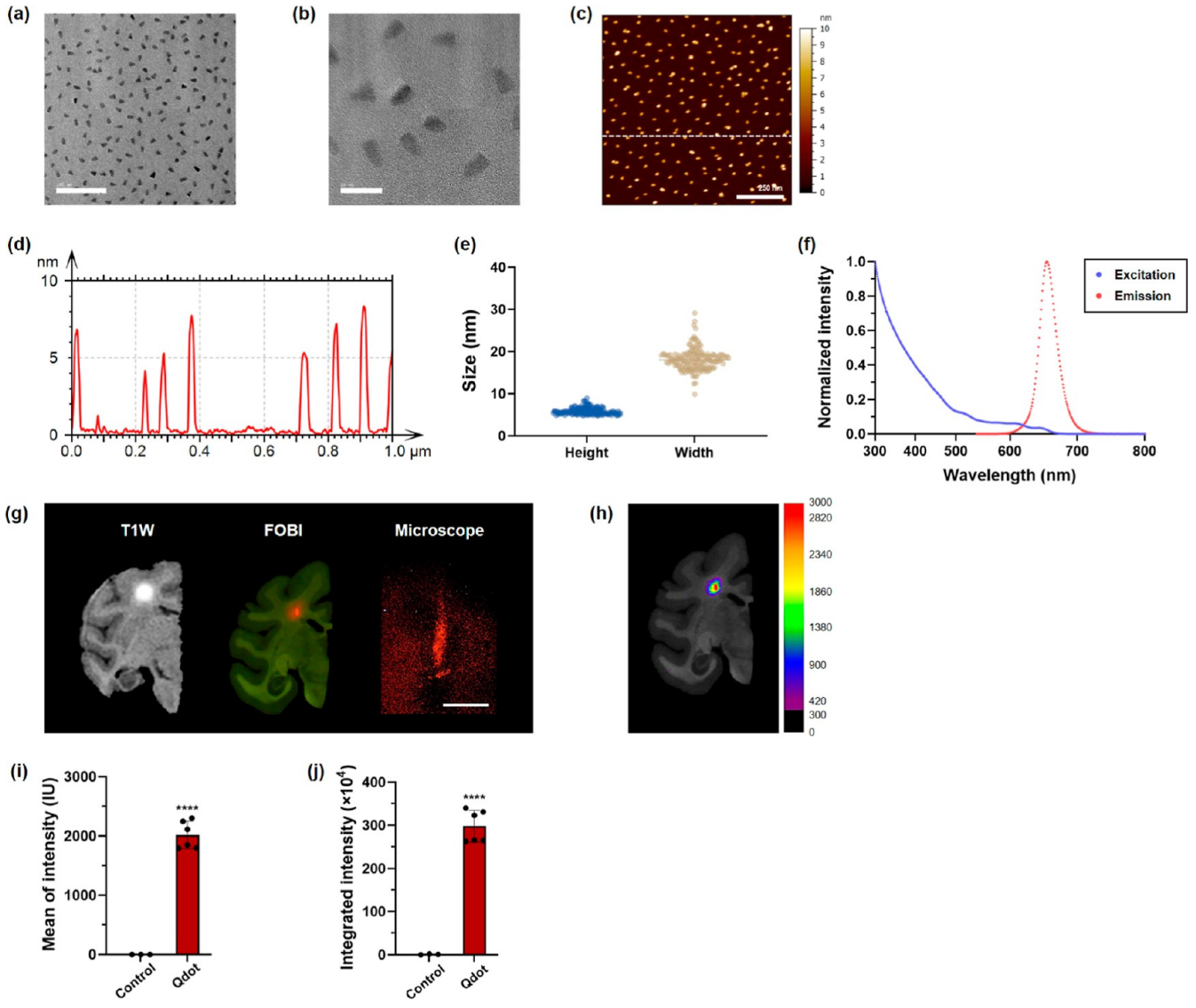


Figure 1. Biodistribution of Qdots in cynomolgus monkeys. Morphological images of CdSe Qdots acquired using TEM (a) scale bar = 100 nm; (b) scale bar = 20 nm and AFM (c) scale bar = 250 nm. (d) Cross-sectional profiles correspond to the dashed line in the topographic AFM image. (e) Particle analysis plots depicting the height and width distribution of samples. (f) Normalized excitation and emission spectra of the Qdots. (g) Follow-up 3.0 T MRI with T1-weighted images, FOBI, and BX51 fluorescence microscope imaging were performed at the subacute stages (1−2 weeks) after Qdot injection. Scale bar = 1 mm. Mean (i) and area-integrated (intensity unit × area) (j) fluorescence intensity measured from the injected site as the region of interest ROI (h) using FOBI. Independent ROIs are presented as mean ± standard deviation. Significant differences were compared to the control using an unpaired *t*-test; ****$p < 0.0001$. Qdot, quantum dot; TEM, transmission electron microscopy; AFM, atomic force microscopy; MRI, magnetic resonance imaging; FOBI, fluorescence-labeled organism bioimaging instrument; IU, intensity unit; ROI, region of interest.

Korea). Scanning was performed in tapping mode to acquire topographic images of each sample. The obtained AFM images, including cross-sectional and particle analyses to measure the height and width of the particles, were analyzed using the MountainsSPIP software (version 9; Digital Surf, France). The analysis included cross-sectional and particle measurements, which resulted in the individual evaluation of the maximum height and width of 150 particles. For transmission electron microscopy (TEM) analysis, the sample was negatively stained with 1% uranyl acetate, and high-resolution images were obtained using FE-TEM (JEOL, Tokyo, Japan) at 200 kV.

2.10. Preparation of Single-Guide RNA. For in vitro RNA transcription, each sense and antisense DNA oligo, designed from SnapGene (GSL Biotech) and purchased from Macrogen (Daejeon, Korea), was mixed with 5 μL T7 RNA polymerase (New England Biolabs, Inc. Beverly, MA, USA), 10 μL 10× RNA polymerase reaction buffer, 2.5 mM each rNTP mix, 10 mM $MgCl_2$, 1 mM dithiothreitol (DTT), 1 μL RNase inhibitor Murine (New England Biolabs), and RNase-free water up to 100 μL and incubated overnight at 37 °C, to generate sgRNAs. After RNA transcription, the reaction mixture was treated with DNase (New England Biolabs) for 30 min at 37 °C. Finally, sgRNAs were purified using the RNeasy MinElute Cleanup kit (Qiagen), and their concentrations were measured using a spectrophotometer (NanoDrop 2000, Thermo Scientific).

2.11. In Vitro DNA Cleavage Assay. In vitro cleavage assessments were conducted with free-Cas9 and Cas9-conjugated Qdots to verify their safe binding with Qdots. DNA fragments containing the target sites (*Rosa26* and *HPRT1*) were prepared using PCR, and three times the molar ratio of the transcribed sgRNA was added to the prepared Cas9 protein (DNA: Cas9: sgRNA molar ratio = 1:3:9) with a complementary sequence to the target site. After combining the target DNA, Cas9 protein, and sgRNA at 37 °C for 1

https://doi.org/10.1021/acsanm.4c04586
ACS Appl. Nano Mater. 2024, 7, 24013−24027

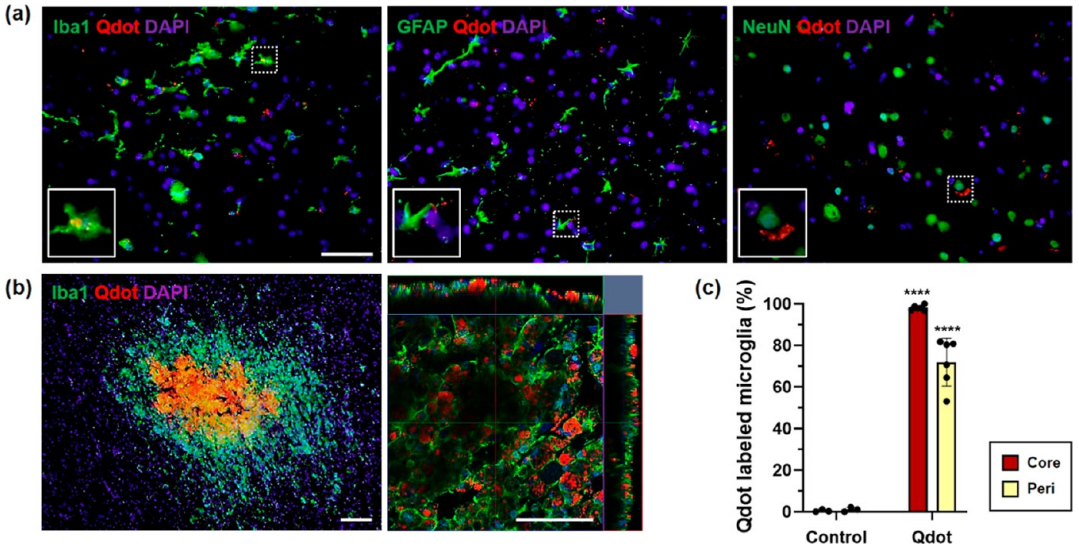


Figure 2. Selective uptake of Qdots by microglia in cynomolgus monkeys. (a) Representative fluorescence microscopy images obtained 2 weeks after Qdot injection. Most Qdots are localized in microglia labeled with anti-Iba1, and they are not taken up by anti-GFAP-labeled astrocytes or anti-NeuN-labeled neurons. Nuclei were stained with DAPI. Scale bar = 50 μm. (b) Representative confocal image of the z-stack. Scale bar = 100 μm. (c) The ratio of Iba1+/Qdot+ cells to total Iba1+ cells quantified in the injection and peri-injection core areas using the ImageJ cell counter. Independent ROIs are presented as mean ± standard deviation. Significant differences were compared to the control using an unpaired *t*-test; ****p < 0.0001. Qdot, quantum dot; Iba1, ionized calcium-binding adapter molecule 1; GFAP, glial fibrillary acidic protein; NeuN, neuronal nuclei; DAPI, 4′,6-diamidino-2-phenylindole; ROI, region of interest.

h, the products of the cleaved DNA were separated using a 1.5% agarose gel.

2.12. Cell Culture and Transfection. BV2 (kindly provided by Dr. Dong-Seok Lee, Kyungpook National University, Daegu, Korea) and HMC3 (CRL-3304; ATCC, Manassas, VA, USA) cells were selected as the microglial cell types. NIH3T3 (CRL-1658; ATCC) and 293FT (R70007; Invitrogen) cells were selected as the nonmicroglial cell type. These cell lines were cultured in Dulbecco's modified Eagle's medium supplemented with 10% fetal bovine serum and 1% penicillin/streptomycin at 37 °C in a humidified atmosphere containing 5% CO_2. One day before transfection, the cells were seeded in 24-well plates at 5 × 10^4 cells/well. For Qdot delivery, 50 μg biotinylated Cas9 protein was mixed with 8 μL Qdots (1000 mM) and up to 500 μL BupH Tris Buffered Saline (Thermo Scientific) per well at room temperature for 2 h. After filtration using Vivaspin 300 K, the Cas9/Qdot solution was incubated with sgRNA (16.7 μg) for 10 min at room temperature. Next, the free-RNP or RNP/Qdot solution was added to the cells in 24-well plates in serum-free medium. After 24 h of incubation at 37 °C, the serum-free medium was replaced with a complete growth medium. For delivery using commercial transfection reagent, 50 μg free-Cas9 protein with 16.7 μg sgRNA was transfected using Lipofectamine 2000, Lipofectamine 3000, CRISPRMAX (Thermo Scientific), and PULSin (Polyplus-transfection Inc., NY, USA), according to the manufacturer's instructions. Cells were harvested 48 h after transfection, and genomic DNA was extracted using the AccuPrep Kit (Bioneer, Daejeon, Korea). To examine the transport mechanism of Cas9/Qdot conjugates, BV2 cells were incubated for 1 h at 37 °C with the following endocytosis inhibitors: chlorpromazine hydrochloride, dynasore hydrate, filipin, nystatin, and cytochalasin D (Sigma-Aldrich). For stability and release evaluation, the conjugates were incubated at 37 °C with 1 mM reduced glutathione (GSH; Santa Cruz Biotechnology, Santa Cruz, CA, USA). After incubation, the remaining Cas9 protein was collected using 300 kDa cutoff filters and quantified using SDS-PAGE analysis.

2.13. Targeted Deep Sequencing. Target regions were amplified from genomic DNA (*Rosa26* and *HPRT1*) using Phusion High-Fidelity DNA Polymerase (New England Biolabs), according to the manufacturer's instructions. Thereafter, the tagged PCR amplicons were subjected to paired-end sequencing using the MiniSeq (Illumina, San Diego, CA, USA). The list of primers used is shown in Supporting Information Table S1. The saved Fastq files were analyzed using a Cas-Analyzer[33] and the indel frequency was calculated.

2.14. Immunocytochemistry. After Cas9 treatment for 48 h, cells were washed with PBS and fixed with 4% PFA for 15 min at room temperature. The fixed cells were permeabilized with 0.3% Triton X-100 for 10 min at room temperature and then blocked for 1 h with 5% normal goat serum, after which they were incubated for 12 h at 4 °C using polyclonal rabbit Guide-it Cas9 (Clontech, Palo Alto, CA, USA). For immunofluorescence, the cells were incubated at room temperature with Alexa Fluor 488 goat antirabbit secondary antibody (Abcam) in the dark for 1 h. Next, the cells were mounted with DAPI VECTASHIELD antifade mounting medium for nuclei counterstaining, and the images were acquired using an Olympus BX51 microscope. The mean fluorescence intensity of Cas9 per cell was quantified using ImageJ software (National Institutes of Health) with an inverted 16 bit.

2.15. Statistical Analysis. Mean values were analyzed using Dunnett's multiple comparisons using one-way analysis of variance (ANOVA) and unpaired *t*-test based on GraphPad Prism (GraphPad Software Inc., San Diego, CA, USA). Differences at a p-value of <0.05 were considered as significant. Data represent the mean ± standard deviation. All graphs were generated and analyzed using GraphPad Prism version 10.1.2.

3. RESULTS AND DISCUSSION

3.1. Characterization and Distribution of Qdots In Vivo. To determine whether CdSe Qdots are selectively taken up by microglia in cynomolgus monkeys and SD rats, we stereotaxically injected Qdots (18.14 ± 2.6 nm width and 5.92 ± 0.8 nm height) (Figure 1a–e), into their frontal white matter. Previous studies have demonstrated that intravenous[34] or intraventricular[35] injection of Qdots exhibits low efficiency for microglia targeting in the brain; therefore, to prevent potential interference with circulating proteins in the blood or cerebrospinal fluid, we opted for direct brain tissue injection. To the best of our knowledge, this is the first preliminary study

https://doi.org/10.1021/acsanm.4c04586
ACS Appl. Nano Mater. 2024, 7, 24013−24027

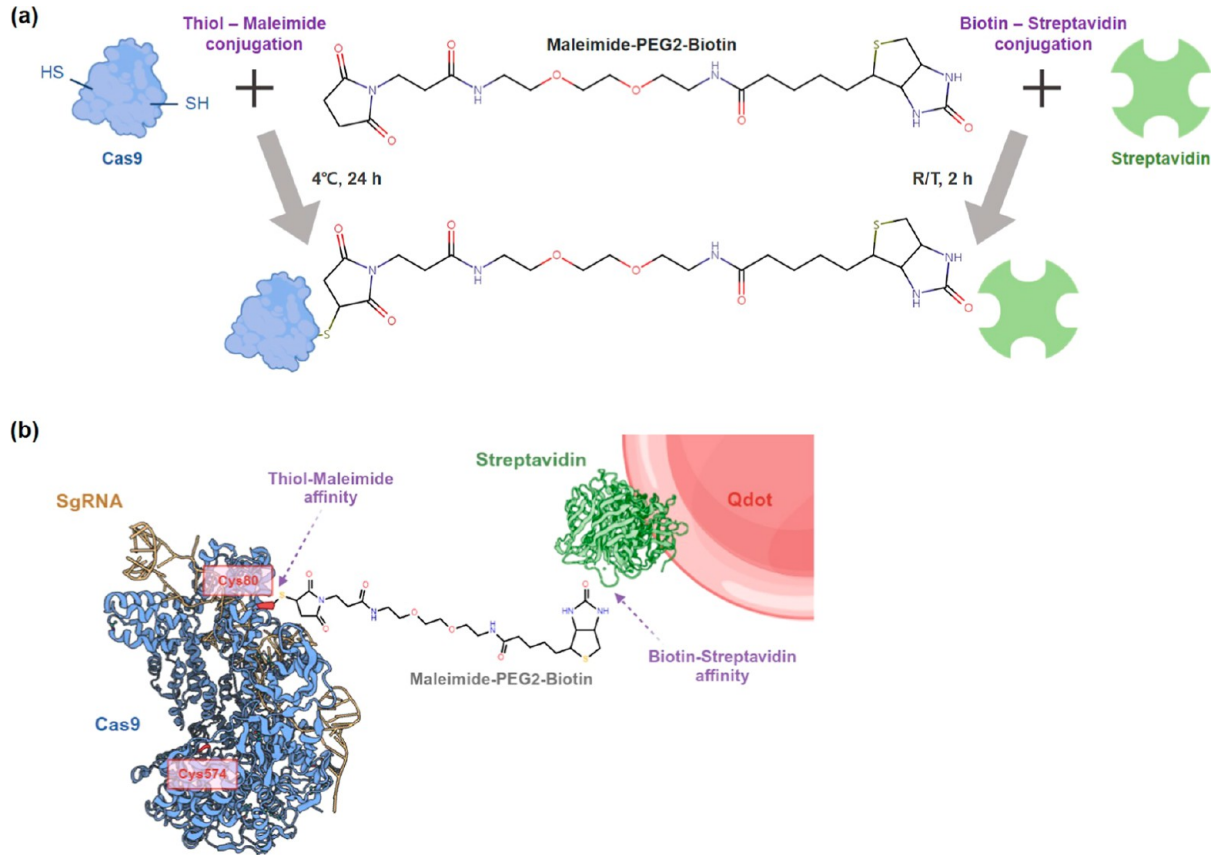


Figure 3. Conjugation of Cas9 ribonucleoprotein to Qdots. (a) Schematic of the preparation of Cas9-conjugated Qdots based on chemical composition. The conjugation was achieved using two types of affinities, thiol-maleimide and biotin−streptavidin, in different circumstances. (b) Conceptual representation of the chemical structure of the conjugates. Cas9 proteins contain two cysteine residues (Cys80 and Cys574). PEG, polyethylene glycol; *R*/*T*, room temperature; Qdot, quantum dot; sgRNA, single guide RNA; Cys, cysteine.

of the brain in nonhuman primates. The excitation and emission spectra of Qdots are shown in Figure 1f. The excitation maximum was measured at a wavelength of 300 nm. Qdots with gadolinium-based MRI contrast agents were trackable on T1-weighted images (Figure 1g). After brain sampling at 1−2 weeks, Qdots were successfully visible at 460 nm using fluorescence devices, such as the FOBI imaging system and a microscope (Figure 1g−j). However, the fluorescence intensity of the Qdots was not detected in the control (Figure 1i,j). As observed in previous studies,[19,28] we demonstrated selective uptake of Qdots by microglia in the brains of cynomolgus monkeys (Figure 2) and SD rats (Supporting Information Figure S1a). The present study also showed that a few Qdots were localized in astrocytes labeled with anti-GFAP or neurons labeled with anti-NeuN (Figures 2a and Supporting Information S1a). However, the microglia-specific localization peaked at the injection areas (98.06 ± 1.2%) when compared to the peri-injection core areas (71.89 ± 11.5%) (Figure 2c).

3.2. Evaluation of Immunological Responses after Qdot Treatment. Next, the expression of pro- and anti-inflammatory cytokines (IL-6, TNF-α, IL-10, and TGF-β) and occurrence of apoptosis (assessed using TUNEL assay) were assessed using histological analyses to evaluate the side effects in cynomolgus monkeys. As shown in Supporting Information Figure S1b−d, the levels of these cytokines and the occurrence of apoptosis in Qdot-treated and control tissues did not differ significantly (IL-6, 18.40 ± 3.5% vs 21.67 ± 2.5%; TNF-α, 15.21 ± 2.9% vs 12.04 ± 1.3%; IL-10, 7.10 ± 1.8% vs 8.21 ± 2.1%; TGF-β, 15.51 ± 2.6% vs 12.99 ± 1.7%; TUNEL, 10.50 ± 2.6% vs 12.93 ± 2.2%). These findings suggest that the injected Qdots did not show inflammatory or toxic triggers. However, in this study, only three cynomolgus monkeys were used, representing a small sample size; therefore, further studies using a large sample size with alternative model organisms are required. Additionally, hematological (Supporting Information Figure S2) and biochemical (Supporting Information Figure S3) assessments for evaluation of the cerebral inflammation[36,37] and complications[38,39] revealed no significant abnormalities in the immune responses when compared to the normal ranges.[31]

Moreover, CdSe Qdots showed no significant effects on viability (Supporting Information Figure S4a,c), microglia-specific endocytosis (Supporting Information Figure S4b), and certain pro- (Supporting Information Figure S4d−i) and anti- (Supporting Information Figure S5) inflammatory mediators in Qdot pretreated (Qdot → LPS) or cotreated (Qdot + LPS) BV2 cells. In particular, Qdots decreased the levels of pro-inflammatory factors, such as NO by 23.05 ± 1.4% (Supporting Information Figure S4d), IL-6 by 17.84 ± 0.8% (Supporting Information Figure S4g), and IL-1β by 55.19 ± 16.3% (Supporting Information Figure S4h) at a high (5 nM) dose, when compared to those induced by LPS only. In contrast, a high dose of Qdot increased the levels of IL-23 (Supporting Information Figure S4i) and several anti-inflammatory cytokines (BDNF, IL-4, IL-13, and IL-25)

https://doi.org/10.1021/acsanm.4c04586
ACS Appl. Nano Mater. 2024, 7, 24013−24027

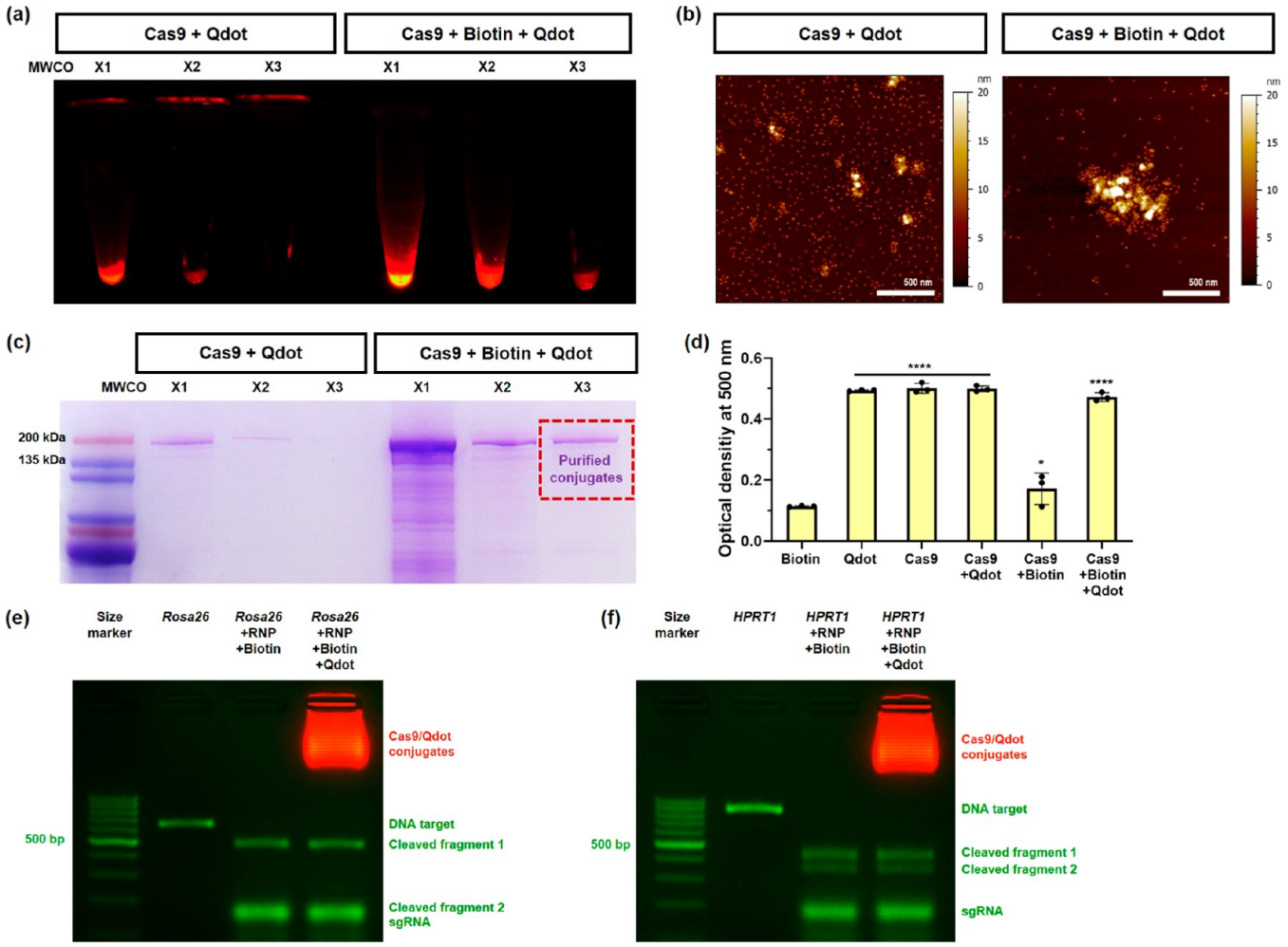


Figure 4. Validation of Cas9/Qdot conjugates. (a−c) Size verification and purification using 300 kDa cutoff filters. Samples with or without maleimide-biotin from the residues visualized using FOBI (a) AFM (b) and SDS-PAGE (c). (d) Biochemical validation of Cas9/Qdot conjugates using the HABA biotin assay. Data are presented as the mean ± standard deviation. $N = 3$ independent HABA samples. *$p < 0.05$, ****$p < 0.0001$ vs free biotin treatment, assessed using one-way ANOVA with Dunnett's multiple comparison test. (e,f) In vitro cleavage assay for activity validation of the Cas9/sgRNA complex after Qdot conjugation. The fragment sizes of cleaved *Rosa26* (f, 617 bp) and *HPRT1* (g, 803 bp) are 474/121 and 431/349 bp, respectively. The size of sgRNA is 96 bp. The red bands indicate Cas9/Qdot conjugates. Treatment with Qdots does not alter the cleavage activity of the Cas9. Qdot, quantum dot; MWCO, molecular weight cutoff; FOBI, fluorescence-labeled organism bioimaging instrument; Qdot, quantum dot; AFM, atomic force microscopy; SDS-PAGE, sodium dodecyl sulfate-polyacrylamide gel electrophoresis; HABA, 4′-hydroxyazobenzene-2-carboxylic acid; sgRNA, single guide RNA; h, hours; *R*/*T*, room temperature.

(Supporting Information Figure S5d−g). Studies have reported the anti-inflammatory functions of carbon dots via reactive oxygen species scavenging[40,41] in mouse macrophages[41,42] and human microvascular endothelial cells.[43] Furthermore, IL-23 is a key factor regulating the functions of IL-17 in inflammatory skin disease,[44] arthritis,[45] and rheumatic diseases.[46] The increased IL-23 levels in this study indicated its role in the acceleration of endocytosis of Qdots[47] or microglial activation via the interferon regulatory transcription factor 5 pathway.[48]

Our studies (Supporting Information Figures S1b−d, S2 and S3) and two nonhuman primate studies[22,23] using histological and hematological data suggest that CdSe Qdots do not cause adverse effects in nonhuman primates. Ye et al. found that components such as cadmium, selenium, and zinc from Qdots showed rapid clearance, slow degradation, and minimal side effects.[22] However, their side effects constitute a highly controversial topic owing to heavy metal-based nanoparticles. Several studies have demonstrated cytotoxicity in ex vivo organotypic whole hemisphere,[49] RAW264.7, and whole blood cell cultures,[50] immortalized brain microvascular endothelial cell lines,[51] BV2 cells, and mice via microglial polarization.[52] Therefore, newly emerging Qdots without heavy metals, such as graphene- or carbon-based Qdots, are required for clinical studies. In particular, graphene Qdots have emerged as promising low-toxicity alternatives for bioengineering applications, such as drug[53] and gene delivery[54] and photoluminescence sensing;[55] nevertheless, they have certain drawbacks. Specifically, graphene Qdots can induce DNA damage due to their nuclear-specific accumulation[56] and exhibit limited fluorescence activity, primarily within the blue to green light range (435−515 nm).[57] Therefore, for stability and efficiency in genome editing and fluorescent tracking, we opted for CdSe Qdots, which demonstrated low toxicity in our in vivo and in vitro studies.

3.3. Preparation and Safety Assessment of Cas9/Qdot Conjugates. Next, we aimed to determine whether Qdots can serve as delivery vectors for microglia-specific gene

https://doi.org/10.1021/acsanm.4c04586
ACS Appl. Nano Mater. 2024, 7, 24013−24027

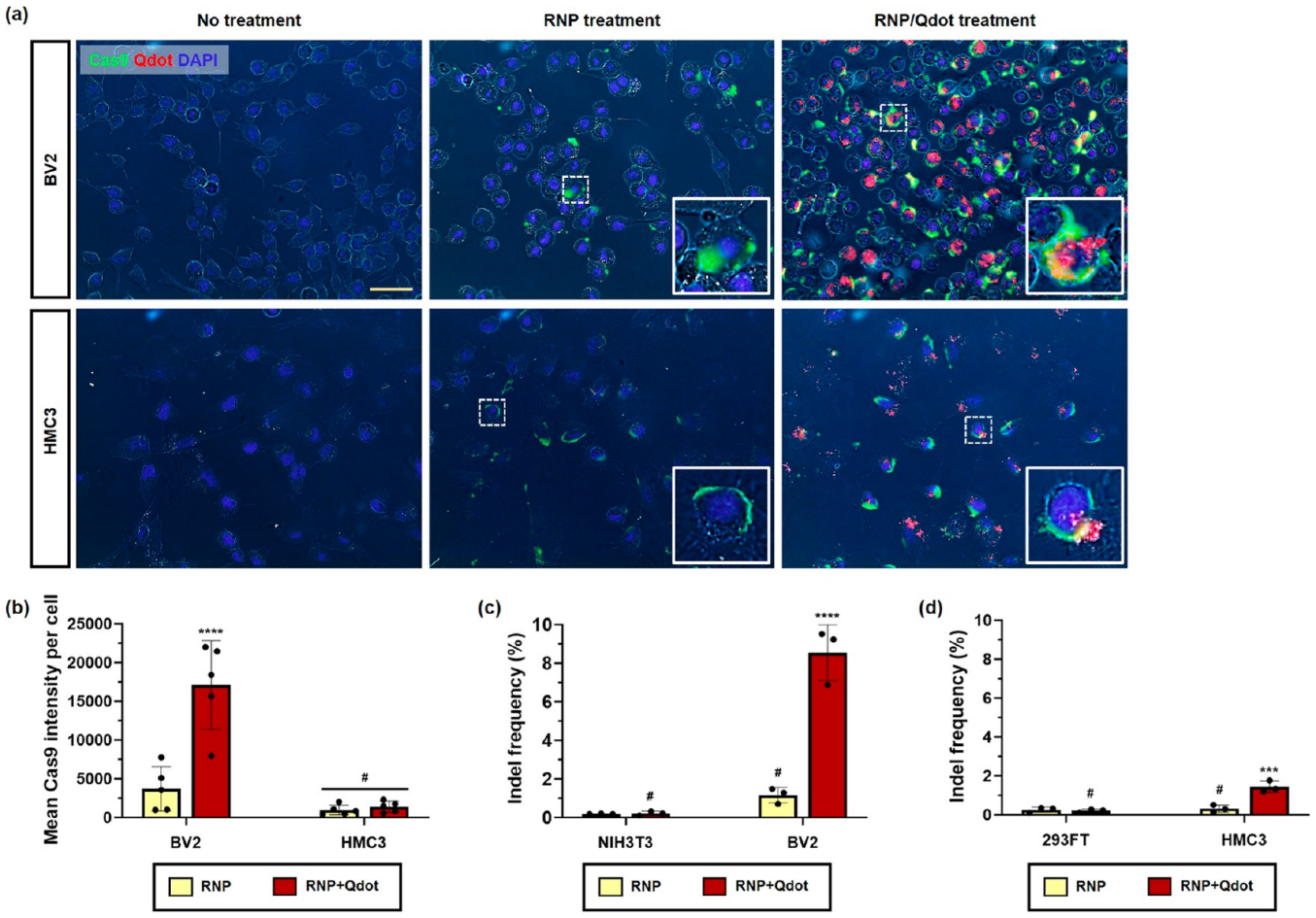


Figure 5. CRISPR-Cas9 mediated gene knockout after delivery using Qdots. (a) Fluorescence microscopy images of BV2 and HMC3 cells treated with free-Cas9 RNPs or RNP/Qdot conjugates, acquired with a 40 × objective. Untreated cells were used as the controls. Nuclei were stained using DAPI. Scale bar = 50 μm. (b) The fluorescence intensity of Cas9 per cell in BV2 and HMC3 cells. Mutation frequencies in *Rosa26* (c) and *HPRT1* (d) targeting Cas9 RNPs in NIH3T3, BV2, 293FT, and HMC3 cells, with or without Qdot conjugation. Mutation frequencies were measured by deep sequencing at 48 h post-transfection. Data are presented as mean ± standard deviation; independent ROIs (b). $^{**}p < 0.01$, $^{***}p < 0.001$, $^{****}p < 0.0001$, # not significant vs free RNP treatment in BV2 (b) NIH3T3 (c) and 293FT (d) cells, assessed using one-way ANOVA with Dunnett's multiple comparisons test. Qdot, quantum dot; CRISPR, clustered regularly interspaced short palindromic repeats; RNP, ribonucleoprotein; DAPI, 4′,6-diamidino-2-phenylindole; h, hours; ROI, region of interest.

editing owing to their selective endocytosis by microglia. Thiol-maleimide and biotin−streptavidin interactions were used to conjugate Cas9 to Qdots, as shown in the scheme in Figure 3. After conjugation, size validation was performed using FOBI (Figure 4a) and SDS-PAGE (Figure 4c). Cas9 has a calculated molecular weight of 154.77 kDa, while Qdot-conjugated Cas9 remained on the 300 kDa cutoff filters. These conjugates were visualized and quantified using AFM (Figures 4b and Supporting Information S6d−h). The Cas9/Qdot conjugates (33.11 ± 57.4 nm width and 6.02 ± 4.2 nm height) showed a distinct distribution when compared to free-Cas9 (8.40 ± 3.6 nm width and 0.32 ± 0.1 nm height) and free-Qdot (18.14 ± 2.6 nm width and 5.92 ± 0.8 nm height), indicating that the combined samples retained the topological characteristics of the individual components, enabling us to differentiate among the three sample types. Subsequently, a biochemical test using the HABA biotin assay confirmed the conjugation (Figure 4d). The assay revealed the nonbinding of conjugates to the HABA-avidin complexes, indicating that the biotin-binding sites were blocked in Cas9 by streptavidin-coated Qdots. Next, we determined the gene editing efficacy of Cas9/Qdot conjugates by targeting major genomic safe harbors, such as mouse *Rosa26* and human *HPRT1*. As shown in Supporting Information Figures S6a,b, purified Cas9 successfully cleaved the *Rosa26* and *HPRT1* amplicons in vitro, and treatment with Qdots did not alter the cleavage activity of Cas9 (Figure 4e,f).

3.4. Gene Knockout Efficiency of Cas9/Qdot Conjugates in Microglia. After verifying the safety of Qdot conjugation, the cells were treated with free-Cas9 RNPs or Cas9/Qdot conjugates (Figure 5a and Supporting Information Figure S7). The findings revealed that Cas9 RNPs did not interfere with microglial labeling by Qdots at 48 h post-transfection. The Qdot delivery system in BV2 cells increased Cas9 fluorescence intensity by 4.6-fold when compared with the nondelivery system (Figure 5b). Moreover, the Qdot delivery system showed higher BV2- (8.54 ± 1.4%) and HMC3- (1.44 ± 0.3%) specific indel frequencies than NIH3T3- (0.22 ± 0.1%)- and 293FT- (0.21 ± 0.1%) specific frequencies (Figure 5c,d). Although commercial reagents, such as Lipofectamine 2000, Lipofectamine 3000, CRISPRMAX, and PULSin exhibited higher mutation efficiency than the Qdot delivery system (Supporting Information Figure S8a−d), microglial specificity was negligible. In addition, these reagents

https://doi.org/10.1021/acsanm.4c04586
ACS Appl. Nano Mater. 2024, 7, 24013−24027

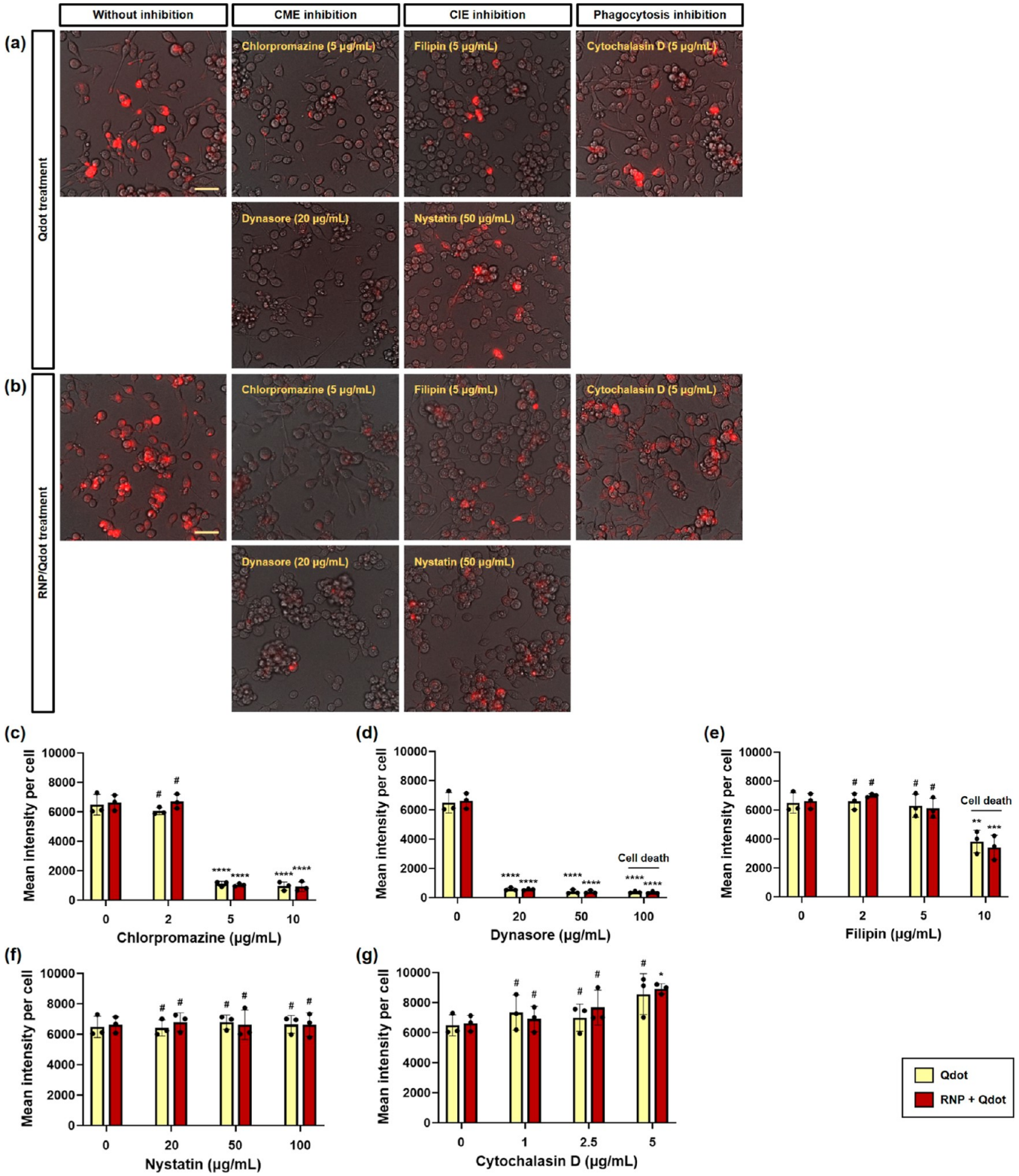


Figure 6. Uptake of RNP/Qdot conjugates by BV2 microglia after endocytosis inhibition. Fluorescence microscopy images of BV2 cells treated with free Qdots (a) or RNP/Qdot conjugates (b) with CME inhibitors (chlorpromazine hydrochloride, dynasore hydrate), CIE inhibitors (filipin, nystatin), and a phagocytosis inhibitor (cytochalasin D). Uninhibited cells were used as controls. Scale bar = 50 μm. (c–g) 594 nm fluorescence intensity per cell with endocytosis inhibitors. Data are presented as mean ± standard deviation. $N = 3$ independent ROIs. *$p < 0.05$, **$p < 0.01$, ***$p < 0.001$, ****$p < 0.0001$, # not significant vs without inhibition; assessed using one-way ANOVA with Dunnett's multiple comparisons test. Qdot, quantum dot; RNP, ribonucleoprotein; CME, clathrin-mediated endocytosis; CIE, clathrin-independent endocytosis; ROI, region of interest.

induced significant cytotoxicity (59.22 ± 6.3%, 67.08 ± 9.0%, 64.07 ± 6.7%, and 34.07 ± 4.2% viability, respectively) when compared to Qdot (87.09 ± 4.7% viability) in BV2 cells at 48 h (Supporting Information Figure S8e).

https://doi.org/10.1021/acsanm.4c04586
ACS Appl. Nano Mater. 2024, 7, 24013−24027

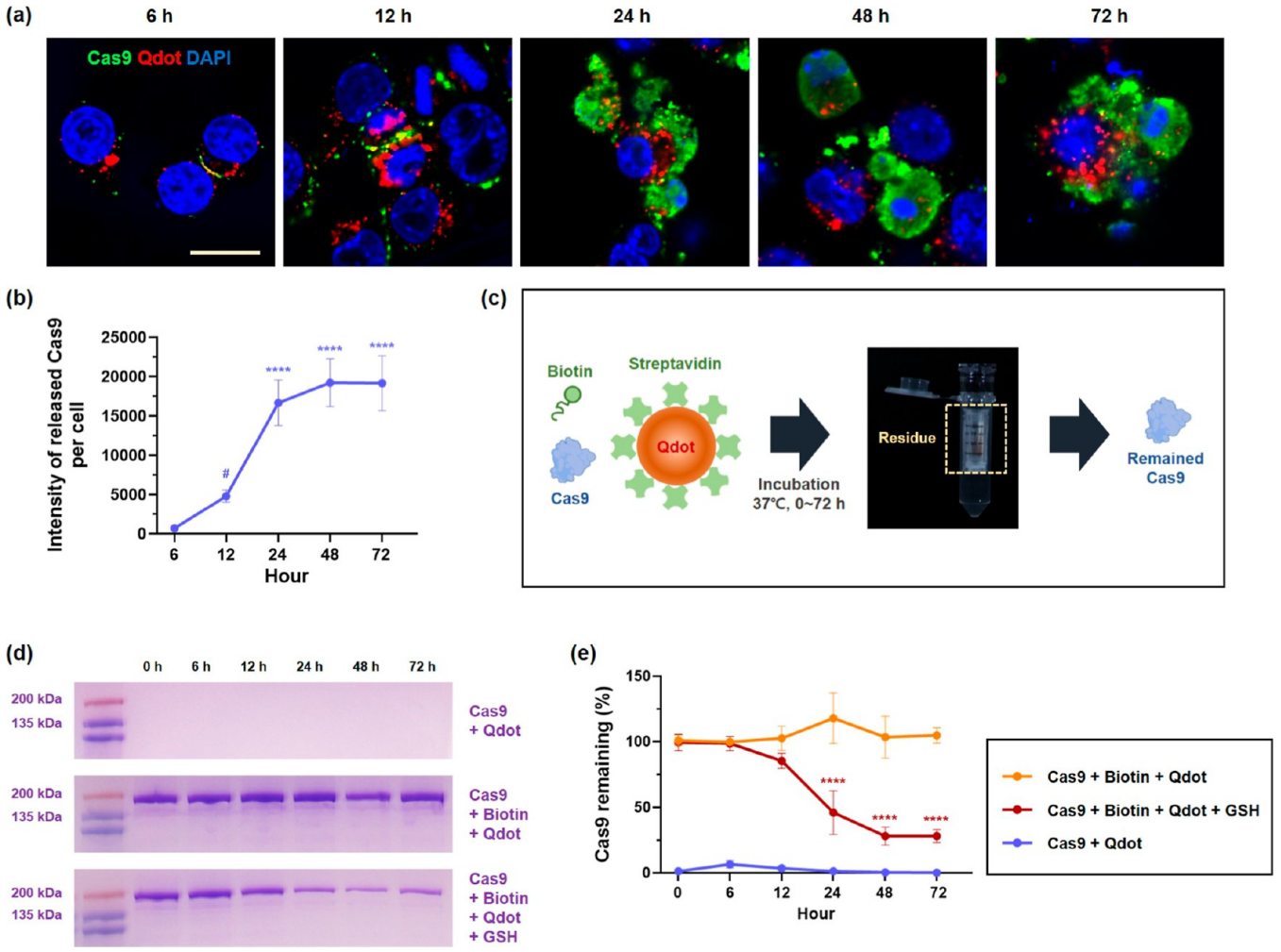


Figure 7. Stability and release of Cas9/Qdot conjugates. (a) Confocal microscopy images of BV2 cells treated with Cas9/Qdot conjugates for 6–72 h. Nuclei were stained with DAPI. Scale bar = 10 μm. (b) Fluorescence intensity of the released Cas9 proteins per cell. (c) In vitro analysis of Cas9 releasing using 300 kDa cutoff filtering. SDS-PAGE analysis (d) and quantification (e) of conjugates containing maleimide-biotin linker or GSH. Data are presented as mean ± standard deviation; N = 5 independent ROIs (b,e). $^{**}p < 0.01$, $^{***}p < 0.001$, $^{****}p < 0.0001$, # not significant vs at 6 h (b) and 0 h (e); assessed using one-way ANOVA with Dunnett's multiple comparisons test. Qdot, quantum dot; DAPI, 4′,6-diamidino-2-phenylindole; h, hours; ROI, regions of interest; GSH, glutathione.

3.5. Transport Mechanism and Intracellular Fate of Cas9/Qdot Conjugates in Microglia. Next, to elucidate the mechanism whereby Cas9/Qdot conjugates are delivered into the cell, we examined the transport mechanism of Cas9/Qdot conjugates within microglia using clathrin-mediated endocytosis (CME) inhibitors (chlorpromazine hydrochloride and dynasore hydrate), clathrin-independent endocytosis (CIE) inhibitors (filipin and nystatin), and a phagocytosis inhibitor (cytochalasin D) (Figure 6). Consistent with a previous study,[19] we observed that the endocytosis of free Qdots (Figure 6a) or Cas9/Qdot conjugates (Figure 6b) selectively decreased after CME inhibition (Figure 6c,d) when compared with that after CIE (Figure 6e,f) and phagocytosis (Figure 6g) inhibition. Cell death was observed after treatment with a high dose of dynasore hydrate (100 μg/mL) or filipin (10 μg/mL). Furthermore, other types of Qdots, such as graphene-,[56,58] Ag_2Se-,[59] carbon-,[41,42,50] CdSeTe-[28] based and PEG-,[19,34] carboxy-[19] functionalized Qdots can be selectively internalized by microglia/macrophages in vitro and in vivo. Therefore, various Qdots can be used for microglia/macrophage-specific gene editing.

In our system, Cas9 proteins were not encapsulated within Qdots, which might expose them vulnerable to degradation by various intrinsic factors. While this surface-conjugation approach simplifies the delivery system and reduces its size, it presents challenges related to protein stability in vivo. In particular, Ruan et al. demonstrated that naked RNPs are susceptible to degradation by proteases and exhibit nonspecific interactions in the bloodstream.[60] To address these issues, we have conducted additional experiments to evaluate the stability of the Cas9/Qdot conjugates using immunofluorescence and SDS-PAGE (Figure 7). The findings revealed that the conjugates were disassembled 24–72 h after delivery, and the released Cas9 proteins were significantly expressed in the cytosol and nucleus (Figure 7a,b). Studies have shown that the maleimide–thiol interaction is unstable in the presence of free thiols, such as GSH, in cells.[61,62] To understand the mechanism of disassembly of the conjugates in reducing environments, we performed further molecular analyses. The findings revealed that Cas9 proteins were released after 300 kDa cutoff filtering (Figure 7c) at 24 h, containing 1 mM reduced GSH at 37 °C (Figure 7d,e). Conversely, Cas9

https://doi.org/10.1021/acsanm.4c04586
ACS Appl. Nano Mater. 2024, 7, 24013−24027

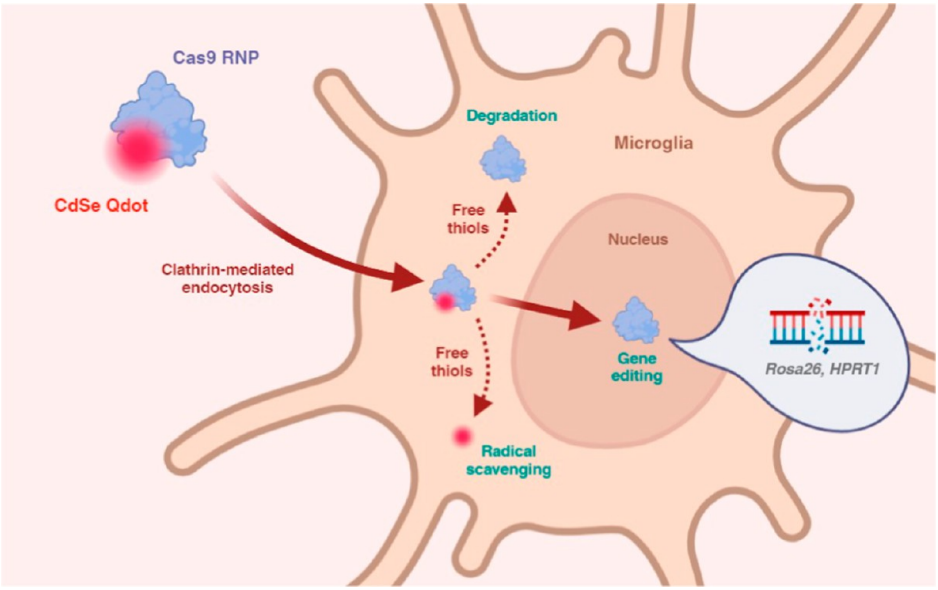


Figure 8. Intracellular fate of Cas9/Qdot conjugates in microglia. The conjugates are released by free thiols (ex. GSH) in the cytoplasm at 24 h after selective internalization by CME. Although disassembled Cas9 proteins are prone to degradation by proteases, they can also pass through the nuclear pore and edit DNA targets (ex. *Rosa26*, *HPRT1*). In addition, the released Qdots can exert anti-inflammatory effects via radical scavenging. Qdot, quantum dot; h, hours; GSH, glutathione; CME, clathrin-mediated endocytosis.

proteins (154.77 kDa) without GSH were retained despite filtering for 72 h at 37 °C due to their conjugation with Qdots (Figure 7d,e). These findings indicated that Qdot could be a pharmacokinetically safe vector without entry or accumulation in the nucleus.

3.6. Alternative Approaches to Improving Gene Editing Efficiency. Given the low mutation efficiency in microglial cells (Figure 5c,d), a histidine-zinc affinity interaction, instead of the biotin−streptavidin affinity, was employed to conjugate Cas9 to the Qdots and reduce the size of the conjugates. As shown in Supporting Information Figure S9a, Cas9 was successfully conjugated to Qdots via self-assembly following previously described protocols.[63,64] After conjugation, size validation was performed using FOBI (Supporting Information Figure S9b) and SDS-PAGE (Supporting Information Figure S9c). We used imidazole as a competitive agent to disrupt histidine-zinc interactions, which revealed that the Qdot-conjugated Cas9 remained on the 300 kDa cutoff filters. However, conjugates with histidine-zinc affinity could not cleave the *Rosa26* and *HPRT1* amplicons (Supporting Information Figure S9d). Alternatively, as SpCas9 proteins have two cysteine residues (Cys80/Cys574),[14] they can form large complexes with each other. Therefore, Cys80 was mutated to serine (C80S) to prevent aggregation. However, no significant differences were observed (Supporting Information Figure S10).

3.7. Limitations and Perspectives of Microglial Modulation Using Qdots. Macrophages, including microglia, contain various cytoplasmic enzymes that degrade foreign proteins or nucleic acids, resulting in resistance to cell transfection.[65] Therefore, many microglial studies have shown low transfection or editing efficiency using commercial reagents, such as Lipofectamine and PULSin. Although Lipofectamine CRISPRMAX is a novel tool for the delivery of Cas9 RNPs, Yu et al. demonstrated lower genome editing efficiencies in macrophage cell lines, such as THP-1 (12%) than in NIH3T3 (57%), 293FT (85%), and HeLa (50%) cells.[66] Moreover, as the majority of transfection reagents cannot perform microglia-specific delivery (Figure S8a−d) or induce cytotoxicity (Supporting Information Figure S8e), we recommend Qdot as a reasonable alternative for microglia-specific genome engineering.

Although we observed microglia-specific gene knockout using Qdot delivery, indel efficiency was very low in animal experiments and clinical studies. We speculate that our conjugation system, which uses the affinity of thiol-maleimide or biotin−streptavidin, has limitations for cell transfection. The reaction of maleimide with cysteine or reactive thiol moieties via the Michael pathway has been applied to antibody-drug conjugates owing to its high selectivity.[61] However, maleimide−thiol structures under physiological conditions with free thiols can become unstable via the retro-Michael pathway.[61] Moreover, under alkaline pH conditions, maleimide can form a hydrolysate that is unreactive toward thiol groups.[67] To stabilize the maleimide−thiol interaction, we used a thiol-free reducing agent (TCEP; Thermo Scientific) and amine- and potassium-free buffer (BupH Tris Buffered Saline; Thermo Scientific). TCEP is widely used as a reducing agent owing to its fast reaction time (less than 5 min), odorless nature, water solubility, and stable structure.[68,69] However, an in situ study reported that TCEP substantially interfered with protein conjugation in the absence of PEG-azides.[70] Therefore, in our study, TCEP was suitably eliminated using a centrifugal filter shortly before binding to maleimide-biotin.

Additionally, because Qdot 655 particles typically have 5−10 streptavidin units, they can irregularly aggregate with Cas9 proteins that are not homologous and are too large to pass through the nuclear pore (Supporting Information Figure S6d−h). Therefore, Carlson-Stevermer et al. used an enzymatically cleavable disulfide linker.[27] They also observed very low gene editing using the biotin−streptavidin affinity. Based on these findings, we speculated that the histidine−zinc interaction could reduce the overall size of the Cas9/Qdot conjugates and prevent their aggregation.[63,64] Histidine−zinc

https://doi.org/10.1021/acsanm.4c04586
ACS Appl. Nano Mater. 2024, 7, 24013−24027

interactions have been utilized to bind various biomolecules, such as maltose-binding protein,[63,64] apo-myoglobin,[63] and cell-penetrating peptide[71] via self-assembly. However, conjugates using this interaction were unable to cleave *Rosa26* and *HPRT1* amplicons (Supporting Information Figure S9). Alkaline borate buffer (pH 9) may affect the structural stability of Cas9 proteins,[72] resulting in lower binding affinity with sgRNAs. Alternatively, as SpCas9 proteins have two cysteine sites (Cys80/Cys574),[14] cysteine point mutations may reduce the size of the conjugates. However, mutated Cas9 (C80S) did not improve editing efficiency (Supporting Information Figure S10).

4. CONCLUSIONS

In summary, we successfully synthesized Qdot and spCas9 RNPs using thiol-maleimide and biotin−streptavidin affinities. These novel conjugates were optimized and verified by fluorescence devices, AFM, SDS-PAGE, and biochemical tests. Consequently, they were selectively internalized by microglia via CME, fluorescently trackable, had low cytotoxicity, and were specifically able to edit the microglial genome (Figure 8). Together, the findings of this study suggest that Qdots could be used as anti-inflammatory vectors against various oxidative stress-mediated diseases or pharmacokinetically safe vectors without entry or accumulation in the nucleus due to their releasing mechanism under reducing environments. However, additional functionalization of Cas9/Qdot conjugates (such as encapsulation and PEG/PEI coating) is needed to increase the efficacy of gene editing.
Complete contact information is available at: https://pubs.acs.org/

■ ASSOCIATED CONTENT

Supporting Information

The Supporting Information is available free of charge at https://pubs.acs.org/doi/10.1021/acsanm.4c04586.

> Safety assessment and selective uptake of microglia by Qdots in vivo; blood test results for Qdot-treated cynomolgus monkeys; In vitro safety assessment of Qdots; purification and size distribution of Cas9/Qdot conjugates; fluorescence microscopy images of Cas9/Qdot-treated microglia; CRISPR-Cas9 mediated gene knockout and cytotoxicity using commercial transfection reagents; Cas9 ribonucleoprotein conjugation to Qdots using a histidine-zinc affinity; CRISPR-Cas9 mediated indel efficiency after point mutation; CRISPR target sequences and PCR primers (PDF)

■ AUTHOR INFORMATION

Corresponding Authors

Youngjeon Lee − *National Primate Research Center, Korea Research Institute of Bioscience and Biotechnology (KRIBB), Cheongju 28116, Republic of Korea; KRIBB School of Bioscience, University of Science and Technology (UST), Daejeon 34113, Republic of Korea;* orcid.org/0000-0002-5387-3441; Email: neurosci@kribb.re.kr

Seung Hwan Lee − *Department of Life Science, Chung-Ang University, Seoul 06974, Republic of Korea;* Email: lsh080390@gmail.com

Authors

Hyeon-Gu Yeo − *National Primate Research Center, Korea Research Institute of Bioscience and Biotechnology (KRIBB), Cheongju 28116, Republic of Korea; KRIBB School of Bioscience, University of Science and Technology (UST), Daejeon 34113, Republic of Korea;* orcid.org/0000-0002-6600-6291

Jinyoung Won − *National Primate Research Center, Korea Research Institute of Bioscience and Biotechnology (KRIBB), Cheongju 28116, Republic of Korea*

Lee Wha Gwon − *National Primate Research Center, Korea Research Institute of Bioscience and Biotechnology (KRIBB), Cheongju 28116, Republic of Korea; KRIBB School of Bioscience, University of Science and Technology (UST), Daejeon 34113, Republic of Korea*

Seokbeom Roh − *Department of Biotechnology and Bioinformatics, Korea University, Sejong 30019, Republic of Korea*

Wi-Jae Lee − *National Primate Research Center, Korea Research Institute of Bioscience and Biotechnology (KRIBB), Cheongju 28116, Republic of Korea; Department of Life Science, Chung-Ang University, Seoul 06974, Republic of Korea*

Kyung Seob Lim − *Futuristic Animal Resource & Research Center, KRIBB, Cheongju 28116, Republic of Korea*

Chang-Yeop Jeon − *National Primate Research Center, Korea Research Institute of Bioscience and Biotechnology (KRIBB), Cheongju 28116, Republic of Korea*

Junghyung Park − *National Primate Research Center, Korea Research Institute of Bioscience and Biotechnology (KRIBB), Cheongju 28116, Republic of Korea*

A Reum Je − *Center for Bio-imaging & Translational Research, Korea Basic Science Institute, Cheongju 28119, Republic of Korea*

Jincheol Seo − *National Primate Research Center, Korea Research Institute of Bioscience and Biotechnology (KRIBB), Cheongju 28116, Republic of Korea*

Jiyeon Cho − *National Primate Research Center, Korea Research Institute of Bioscience and Biotechnology (KRIBB), Cheongju 28116, Republic of Korea*

Jung Bae Seong − *National Primate Research Center, Korea Research Institute of Bioscience and Biotechnology (KRIBB), Cheongju 28116, Republic of Korea*

Yu Gyeong Kim − *National Primate Research Center, Korea Research Institute of Bioscience and Biotechnology (KRIBB), Cheongju 28116, Republic of Korea; KRIBB School of Bioscience, University of Science and Technology (UST), Daejeon 34113, Republic of Korea;* orcid.org/0000-0003-4907-3756

Keonwoo Kim − *National Primate Research Center, Korea Research Institute of Bioscience and Biotechnology (KRIBB), Cheongju 28116, Republic of Korea; School of Life Sciences, BK21 Plus KNU Creative BioResearch Group, Kyungpook National University, Daegu 41566, Republic of Korea*

Sangwoo Lee − *National Primate Research Center, Korea Research Institute of Bioscience and Biotechnology (KRIBB), Cheongju 28116, Republic of Korea; Department of Biotechnology and Bioinformatics, Korea University, Sejong 30019, Republic of Korea*

Sung-hyun Park − *National Primate Research Center, Korea Research Institute of Bioscience and Biotechnology (KRIBB), Cheongju 28116, Republic of Korea*

https://doi.org/10.1021/acsanm.4c04586
ACS Appl. Nano Mater. 2024, 7, 24013−24027

Won Seok Choi − *National Primate Research Center, Korea Research Institute of Bioscience and Biotechnology (KRIBB), Cheongju 28116, Republic of Korea*
Yang Hoon Huh − *Center for Bio-imaging & Translational Research, Korea Basic Science Institute, Cheongju 28119, Republic of Korea*
Gyudo Lee − *Department of Biotechnology and Bioinformatics, Korea University, Sejong 30019, Republic of Korea;* orcid.org/0000-0001-7895-5112
Hyoung-Chin Kim − *Laboratory Animal Resource & Research Center, KRIBB, Cheongju 28116, Republic of Korea*

Complete contact information is available at: https://pubs.acs.org/10.1021/acsanm.4c04586

Author Contributions

○H.-G.Y., J.W. and L.W.G. contributed equally to this work. All the authors contributed toward writing the manuscript and have approved the final version of the manuscript.

Notes

The authors declare no competing financial interest.

■ ACKNOWLEDGMENTS

This work was supported by the Korea Research Institute of Bioscience and Biotechnology (KRIBB) Research Initiative Program (KGM4562431, KGM5282423), the National Research Foundation funded by the Korean Ministry of Education, Science, and Technology (NRF-2022R1A2C4001609), the Ministry of Science and ICT (NRF-2022M3H9A2096197), the Korea Basic Science Institute R&D program (C410000), and the University of Science and Technology (UST) Young Scientist + Research Program 2023 (2023YS07, KFM0652311). The authors acknowledge the schematic illustrations from BioRender.com, spectral data from Chroma Technology (Bellows Falls, VT, US), and chemical structures (doi.org/10.2210/pdb 4ZT0/pdb and doi.org/10.2210/pdb 5N8E/pdb) from the RCSB Protein Data Bank web portal (rcsb.org), and a supplementary cover graphic created by Jeongung Cho (3D Morph).

■ ABBREVIATIONS

CdSe, cadmium selenide; CRISPR, clustered regularly interspaced short palindromic repeats; DAPI, 4′,6-diamidino-2-phenylindole; FOBI, fluorescence-labeled organism bioimaging instrument; GFAP, glial fibrillary acidic protein; GSH, glutathione; HABA, 4′-hydroxyazobenzene-2-carboxylic acid; IBA1, ionized calcium-binding adapter molecule 1; IFN-γ, interferon gamma; IGF-1, insulin like growth factor-1; IL-1β, interleukin-1 beta; LPS, lipopolysaccharide; MCP-1, monocyte chemoattractant protein-1; MRI, magnetic resonance imaging; NeuN, neuronal nuclei; NO, nitric oxide; Qdot, quantum dot; RNPs, ribonucleoproteins; sgRNA, single guide RNA; TGF-β, transforming growth factor-beta; TNF-α, tumor necrosis factor alpha

■ REFERENCES

(1) Lawson, L. J.; Perry, V. H.; Gordon, S. Turnover of resident microglia in the normal adult mouse brain. *Neuroscience* **1992**, *48*, 405−415.
(2) Muzio, L.; Viotti, A.; Martino, G. Microglia in Neuroinflammation and Neurodegeneration: From Understanding to Therapy. *Front Neurosci* **2021**, *15*, 742065.
(3) Lee, Y.; Lee, S.-R.; Choi, S.-S.; Yeo, H.-G.; Chang, K.-T.; Lee, H.-J. Therapeutically targeting neuroinflammation and microglia after acute ischemic stroke. *BioMed Res. Int.* **2014**, *2014*, 297241.
(4) Guo, S.; Wang, H.; Yin, Y. Microglia Polarization From M1 to M2 in Neurodegenerative Diseases. *Front. Aging Neurosci.* **2022**, *14*, 815347.
(5) Nakagawa, Y.; Chiba, K. Role of microglial m1/m2 polarization in relapse and remission of psychiatric disorders and diseases. *Pharmaceuticals* **2014**, *7*, 1028−1048.
(6) Boehler, R.-M.; Kuo, R.; Shin, S.; Goodman, A.; Pilecki, M.; Leonard, J.; Shea, L. Lentivirus delivery of IL-10 to promote and sustain macrophage polarization towards an anti-inflammatory phenotype. *Biotechnol. Bioeng.* **2014**, *111*, 1210−1221.
(7) Ganbold, T.; Bao, Q.; Zandan, J.; Hasi, A.; Baigude, H. Modulation of Microglia Polarization through Silencing of NF-κB p65 by Functionalized Curdlan Nanoparticle-Mediated RNAi. *ACS Appl. Mater. Interfaces* **2020**, *12*, 11363−11374.
(8) Kawabori, M.; Kacimi, R.; Kauppinen, T.; Calosing, C.; Kim, J.-Y.; Hsieh, C.-L.; Nakamura, M.-C.; Yenari, M.-A. Triggering receptor expressed on myeloid cells 2 (TREM2) deficiency attenuates phagocytic activities of microglia and exacerbates ischemic damage in experimental stroke. *J. Neurosci.* **2015**, *35*, 3384−3396.
(9) Shi, W.; Wei, X.; Wang, Z.; Han, H.; Fu, Y.; Liu, J.; Zhang, Y.; Guo, J.; Dong, C.; Zhou, D.; et al. HDAC9 exacerbates endothelial injury in cerebral ischaemia/reperfusion injury. *J. Cell. Mol. Med.* **2016**, *20*, 1139−1149.
(10) Lin, R.; Zhou, Y.; Yan, T.; Wang, R.; Li, H.; Wu, Z.; Zhang, X.; Zhou, X.; Zhao, F.; Zhang, L.; et al. Directed evolution of adeno-associated virus for efficient gene delivery to microglia. *Nat. Methods* **2022**, *19*, 976−985.
(11) McQuade, A.; Kang, Y.-J.; Hasselmann, J.; Jairaman, A.; Sotelo, A.; Coburn, M.; Shabestari, S.-K.; Chadarevian, J.-P.; Fote, G.; Tu, C.-H.; et al. Gene expression and functional deficits underlie TREM2-knockout microglia responses in human models of Alzheimer's disease. *Nat. Commun.* **2020**, *11*, 5370.
(12) Raikwar, S.-P.; Thangavel, R.; Dubova, I.; Selvakumar, G.-P.; Ahmed, M.-E.; Kempuraj, D.; Zaheer, S.-A.; Iyer, S.-S.; Zaheer, A. Targeted Gene Editing of Glia Maturation Factor in Microglia: a Novel Alzheimer's Disease Therapeutic Target. *Mol. Neurobiol.* **2019**, *56*, 378−393.
(13) Pearson-Leary, J.; Osborne, D. M.; McNay, E. C. Role of Glia in Stress-Induced Enhancement and Impairment of Memory. *Front Integr Neurosci* **2016**, *9*, 63.
(14) Globyte, V.; Lee, S. H.; Bae, T.; Kim, J. S.; Joo, C. CRISPR/Cas9 searches for a protospacer adjacent motif by lateral diffusion. *EMBO J.* **2019**, *38*, No. e99466.
(15) Xu, C.; Lu, Z.; Luo, Y.; Liu, Y.; Cao, Z.; Shen, S.; Li, H.; Liu, J.; Chen, K.; Chen, Z.; et al. Targeting of NLRP3 inflammasome with gene editing for the amelioration of inflammatory diseases. *Nat. Commun.* **2018**, *9*, 4092.
(16) Wei, T.; Cheng, Q.; Min, Y. L.; Olson, E. N.; Siegwart, D. J. Systemic nanoparticle delivery of CRISPR-Cas9 ribonucleoproteins for effective tissue specific genome editing. *Nat. Commun.* **2020**, *11*, 3232.
(17) Swiech, L.; Heidenreich, M.; Banerjee, A.; Habib, N.; Li, Y.; Trombetta, J.; Sur, M.; Zhang, F. In vivo interrogation of gene function in the mammalian brain using CRISPR-Cas9. *Nat. Biotechnol.* **2015**, *33*, 102−106.
(18) Lee, B.; Lee, K.; Panda, S.; Gonzales-Rojas, R.; Chong, A.; Bugay, V.; Park, H.-M.; Brenner, R.; Murthy, N.; Lee, H.-Y. Nanoparticle delivery of CRISPR into the brain rescues a mouse model of fragile X syndrome from exaggerated repetitive behaviours. *Nat. Biomed. Eng.* **2018**, *2*, 497−507.
(19) Minami, S.-S.; Sun, B.; Popat, K.; Kauppinen, T.; Pleiss, M.; Zhou, Y.; Ward, M.-E.; Floreancig, P.; Mucke, L.; Desai, T.; et al. Selective targeting of microglia by quantum dots. *J. Neuroinflammation* **2012**, *9*, 22.
(20) Walling, M. A.; Novak, J. A.; Shepard, J. R. E. Quantum dots for live cell and in vivo imaging. *Int. J. Mol. Sci.* **2009**, *10*, 441−491.

(21) Hotz, C. Z. Applications of quantum dots in biology: an overview. *NanoBiotechnology* **2005**, *303*, 1−17.
(22) Ye, L.; Yong, K.-T.; Liu, L.; Roy, I.; Hu, R.; Zhu, J.; Cai, H.; Law, W.-C.; Liu, J.; Wang, K.; et al. A pilot study in non-human primates shows no adverse response to intravenous injection of quantum dots. *Nat. Nanotechnol.* **2012**, *7*, 453−458.
(23) Liu, J.; Erogbogbo, F.; Yong, K.-T.; Ye, L.; Liu, J.; Hu, R.; Chen, H.; Hu, Y.; Yang, Y.; Yang, J.; et al. Assessing clinical prospects of silicon quantum dots: studies in mice and monkeys. *ACS Nano* **2013**, *7*, 7303−7310.
(24) Zhai, L.-M.; Zhao, Y.; Xiao, R.-L.; Zhang, S.-Q.; Tian, B.-H.; Li, X.-X.; Zhang, R.; Ma, R.-S.; Liang, H.-X. Nuclear-targeted carbon quantum dot mediated CRISPR/Cas9 delivery for fluorescence visualization and efficient editing. *Nanoscale* **2022**, *14*, 14645−14660.
(25) Yue, H.; Zhou, X.; Cheng, M.; Xing, D. Graphene oxide-mediated Cas9/sgRNA delivery for efficient genome editing. *Nanoscale* **2018**, *10*, 1063−1071.
(26) Oostendorp, M.; Douma, K.; Hackeng, T.-M.; Dirksen, A.; Post, M.-J.; van Zandvoort, M.-A.; Backes, W.-H. Quantitative molecular magnetic resonance imaging of tumor angiogenesis using cNGR-labeled paramagnetic quantum dots. *Cancer Res.* **2008**, *68*, 7676−7683.
(27) Carlson-Stevermer, J.; Abdeen, A.-A.; Kohlenberg, L.; Goedland, M.; Molugu, K.; Lou, M.; Saha, K. Assembly of CRISPR ribonucleoproteins with biotinylated oligonucleotides via an RNA aptamer for precise gene editing. *Nat. Commun.* **2017**, *8*, 1711.
(28) Sugiyama, T.; Kuroda, S.; Osanai, T.; Shichinohe, H.; Kuge, Y.; Ito, M.; Kawabori, M.; Iwasaki, Y. Near-infrared fluorescence labeling allows noninvasive tracking of bone marrow stromal cells transplanted into rat infarct brain. *Neurosurgery* **2011**, *68*, 1036−1047.
(29) England, T.-J.; Sprigg, N.; Alasheev, A.-M.; Belkin, A.-A.; Kumar, A.; Prasad, K.; Bath, P.-M. Granulocyte-Colony Stimulating Factor (G-CSF) for stroke: an individual patient data meta-analysis. *Sci. Rep.* **2016**, *6*, 36567.
(30) Percie du Sert, N.; et al. The ARRIVE guidelines 2.0: updated guidelines for reporting animal research. *BMJ. Open Sci.* **2020**, *4*, No. e100115.
(31) Koo, B.-S.; Lee, D.-H.; Kang, P.; Jeong, K.-J.; Lee, S.; Kim, K.; Lee, Y.; Huh, J.-W.; Kim, Y.-H.; Park, S.-J.; et al. Reference values of hematological and biochemical parameters in young-adult cynomolgus monkey (Macaca fascicularis) and rhesus monkey (Macaca mulatta) anesthetized with ketamine hydrochloride. *Lab. Anim. Res.* **2019**, *35*, 7.
(32) Kim, H.; Lee, W.-j.; Oh, Y.; Kang, S.-H.; Hur, J.-K.; Lee, H.; Song, W.; Lim, K.-S.; Park, Y.-H.; Song, B.-S.; et al. Enhancement of target specificity of CRISPR-Cas12a by using a chimeric DNA-RNA guide. *Nucleic Acids Res.* **2020**, *48*, 8601−8616.
(33) Park, J.; Lim, K.; Kim, J. S.; Bae, S. Cas-analyzer: an online tool for assessing genome editing results using NGS data. *Bioinformatics* **2017**, *33*, 286−288.
(34) Choi, A. O.; Maysinger, D. Intranasal Fluorescent Nanocrystals for Longitudinal In Vivo Evaluation of Cerebral Microlesions. *Pharm. Nanotechnol.* **2013**, *1*, 93−104.
(35) Varela, J.-A.; Dupuis, J.-P.; Etchepare, L.; Espana, A.; Cognet, L.; Groc, L. Targeting neurotransmitter receptors with nanoparticles in vivo allows single-molecule tracking in acute brain slices. *Nat. Commun.* **2016**, *7*, 10947.
(36) Guo, Y.; Chen, J.; Ji, W.; Xu, L.; Xie, Y.; He, S.; Lai, C.; Hou, K.; Li, Z.; Chen, G.; et al. High-titer AAV disrupts cerebrovascular integrity and induces lymphocyte infiltration in adult mouse brain. *Mol. Ther.–Methods Clin. Dev.* **2023**, *31*, 101102.
(37) Sharma, H. S.; Hussain, S.; Schlager, J.; Ali, S. F.; Sharma, A. Influence of Nanoparticles on Blood−Brain Barrier Permeability and Brain Edema Formation in Rats. *Acta Neurochir., Suppl.* **2010**, *106*, 359−364.
(38) Das, S.-K.; Sen, K.; Ghosh, B.; Ghosh, N.; Sinha, K.; Sil, P.-C. Molecular mechanism of nanomaterials induced liver injury: A review. *World J. Hepatol* **2024**, *16*, 566−600.
(39) Dabir, S.; Mohammad-Taheri, Z.; Parsa, T.; Abbasi-Nazari, M.; Radpay, B.; Radmand, G. Effects of propofol versus isoflurane on liver function after open thoracotomy. *Asian Cardiovasc. Thorac. Ann.* **2015**, *23*, 292−298.
(40) Das, B.; Dadhich, P.; Pal, P.; Srivas, P.-K.; Bankoti, K.; Dhara, S. Carbon nanodots from date molasses: new nanolights for the in vitro scavenging of reactive oxygen species. *J. Mater. Chem. B* **2014**, *2*, 6839−6847.
(41) Wang, H.; Zhang, M.; Ma, Y.; Wang, B.; Huang, H.; Liu, Y.; Shao, M.; Kang, Z. Carbon Dots Derived from Citric Acid and Glutathione as a Highly Efficient Intracellular Reactive Oxygen Species Scavenger for Alleviating the Lipopolysaccharide-Induced Inflammation in Macrophages. *ACS Appl. Mater. Interfaces* **2020**, *12*, 41088−41095.
(42) Yang, C.; Ogaki, R.; Hansen, L.; Kjems, J.; Teo, B. M. Theranostic carbon dots derived from garlic with efficient anti-oxidative effects towards macrophages. *RSC Adv.* **2015**, *5*, 97836−97840.
(43) Belperain, S.; Kang, Z.-Y.; Dunphy, A.; Priebe, B.; Chiu, N.-H.-L.; Jia, Z. Anti-Inflammatory Effect and Cellular Uptake Mechanism of Carbon Nanodots in in Human Microvascular Endothelial Cells. *Nanomater.* **2021**, *11*, 1247.
(44) Liu, T.; Li, S.; Ying, S.; Tang, S.; Ding, Y.; Li, Y.; Qiao, J.; Fang, H. The IL-23/IL-17 Pathway in Inflammatory Skin Diseases: From Bench to Bedside. *Front Immunol* **2020**, *11*, 594735.
(45) Lubberts, E. Erratum: The IL-23−IL-17 axis in inflammatory arthritis. *Nat. Rev. Rheumatol* **2015**, *11*, 562.
(46) Schinocca, C.; Rizzo, C.; Fasano, S.; Grasso, G.; La Barbera, L.; Ciccia, F.; Guggino, G. Role of the IL-23/IL-17 Pathway in Rheumatic Diseases: An Overview. *Front Immunol* **2021**, *12*, 637829.
(47) Stark, M.-A.; Huo, Y.; Burcin, T.-L.; Morris, M.-A.; Olson, T.-S.; Ley, K. Phagocytosis of apoptotic neutrophils regulates granulopoiesis via IL-23 and IL-17. *Immunity* **2005**, *22*, 285−294.
(48) Chen, S.; Saeed, A.-F.; Liu, Q.; Jiang, Q.; Xu, H.; Xiao, G.-G.; Rao, L.; Duo, Y. Macrophages in immunoregulation and therapeutics. *Signal Transduction Targeted Ther.* **2023**, *8*, 207.
(49) Zhang, M.; Bishop, B.-P.; Thompson, N.-L.; Hildahl, K.; Dang, B.; Mironchuk, O.; Chen, N.; Aoki, R.; Holmberg, V.-C.; Nance, E. Quantum Dot Cellular Uptake and Toxicity in the Developing Brain: Implications for Use as Imaging Probes. *Nanoscale Adv.* **2019**, *1*, 3424−3442.
(50) Lategan, K.; Fowler, J.; Bayati, M.; Fidalgo de Cortalezzi, M.; Pool, E. The Effects of Carbon Dots on Immune System Biomarkers, Using the Murine Macrophage Cell Line RAW 264.7 and Human Whole Blood Cell Cultures. *Nanomaterials* **2018**, *8*, 388.
(51) Kania, K. D.; Wagner, W.; Pulaski, L. CdSe/ZnS Core-Shell-Type Quantum Dot Nanoparticles Disrupt the Cellular Homeostasis in Cellular Blood-Brain Barrier Models. *Int. J. Mol. Sci.* **2021**, *22*, 1068.
(52) He, K.; Liang, X.; Wei, T.; Liu, N.; Wang, Y.; Zou, L.; Bai, C.; Yao, Y.; Wu, T.; Kong, L.; et al. A metabolomics study: CdTe/ZnS quantum dots induce polarization in mice microglia. *Chemosphere* **2020**, *246*, 125629.
(53) Zhao, C.; Song, X.; Liu, Y.; Fu, Y.; Ye, L.; Wang, N.; Wang, F.; Li, L.; Mohammadniaei, M.; Zhang, M.; et al. Synthesis of graphene quantum dots and their applications in drug delivery. *J. Nanobiotechnol.* **2020**, *18*, 142.
(54) Ghafary, S. M.; Nikkhah, M.; Hatamie, S.; Hosseinkhani, S. Simultaneous Gene Delivery and Tracking through Preparation of Photo-Luminescent Nanoparticles Based on Graphene Quantum Dots and Chimeric Peptides. *Sci. Rep.* **2017**, *7*, 9552.
(55) Kumawat, M. K.; Thakur, M.; Gurung, R. B.; Srivastava, R. Graphene Quantum Dots for Cell Proliferation, Nucleus Imaging, and Photoluminescent Sensing Applications. *Sci. Rep.* **2017**, *7*, 15858.
(56) Xu, L.; Dai, Y.; Wang, Z.; Zhao, J.; Li, F.; White, J. C.; Xing, B. Graphene quantum dots in alveolar macrophage: uptake-exocytosis, accumulation in nuclei, nuclear responses and DNA cleavage. *Part Fibre Toxicol* **2018**, *15*, 45.
(57) Zhang, Q.; Tao, Y.; Tang, B.; Yang, J.; Liang, H.; Wang, B.; Wang, J.; Jiang, X.; Ji, L.; Li, S. Graphene Quantum Dots with

Improved Fluorescence Activity via Machine Learning: Implications for Fluorescence Monitoring. *ACS Appl. Nano Mater.* **2022**, *5*, 2728−2737.
(58) Liang, X.; Wu, T.; Tang, M. Microarray analysis of gene expression differences in microglia after exposure to graphene quantum dots. *Sci. Total Environ.* **2020**, *749*, 141385.
(59) Wu, T.; Liang, X.; He, K.; Wei, T.; Wang, Y.; Zou, L.; Bai, C.; Liu, N.; Zhang, T.; Xue, Y.; et al. The role of NLRP3 inflammasome activation in the neuroinflammatory responses to Ag(2)Se quantum dots in microglia. *Nanoscale* **2019**, *11*, 20820−20836.
(60) Ruan, W.; Jiao, M.; Xu, S.; Ismail, M.; Xie, X.; An, Y.; Guo, H.; Qian, R.; Shi, B.; Zheng, M. Brain-targeted CRISPR/Cas9 nanomedicine for effective glioblastoma therapy. *J. Controlled Release* **2022**, *351*, 739−751.
(61) Huang, W.; Wu, X.; Gao, X.; Yu, Y.; Lei, H.; Zhu, Z.; Shi, Y.; Chen, Y.; Qin, M.; Wang, W.; et al. Maleimide-thiol adducts stabilized through stretching. *Nat. Chem.* **2019**, *11*, 310−319.
(62) Baldwin, A. D.; Kiick, K. L. Reversible maleimide-thiol adducts yield glutathione-sensitive poly(ethylene glycol)-heparin hydrogels. *Polym. Chem.* **2013**, *4*, 133−143.
(63) Goldman, E.-R.; Medintz, I.-L.; Hayhurst, A.; Anderson, G.-P.; Mauro, J.; Iverson, B.-L.; Georgiou, G.; Mattoussi, H. Self-assembled luminescent CdSe−ZnS quantum dot bioconjugates prepared using engineered poly-histidine terminated proteins. *Anal. Chim. Acta* **2005**, *534*, 63−67.
(64) Medintz, I.-L.; Clapp, A.-R.; Mattoussi, H.; Goldman, E.-R.; Fisher, B.; Mauro, J.-M. Self-assembled nanoscale biosensors based on quantum dot FRET donors. *Nat. Mater.* **2003**, *2*, 630−638.
(65) Smolders, S.; Kessels, S.; Smolders, S.-M.-T.; Poulhes, F.; Zelphati, O.; Sapet, C.; Brône, B. Magnetofection is superior to other chemical transfection methods in a microglial cell line. *J. Neurosci Methods* **2018**, *293*, 169−173.
(66) Yu, X.; Liang, X.; Xie, H.; Kumar, S.; Ravinder, N.; Potter, J.; de Mollerat du Jeu, X.; Chesnut, J.-D. Improved delivery of Cas9 protein/gRNA complexes using lipofectamine CRISPRMAX. *Biotechnol. Lett.* **2016**, *38*, 919−929.
(67) Martinez-Jothar, L.; Doulkeridou, S.; Schiffelers, R.-M.; Sastre Torano, J.; Oliveira, S.; van Nostrum, C.-F.; Hennink, W.-E. Insights into maleimide-thiol conjugation chemistry: Conditions for efficient surface functionalization of nanoparticles for receptor targeting. *J. Controlled Release* **2018**, *282*, 101−109.
(68) Han, J. C.; Han, G. Y. A procedure for quantitative determination of tris(2-carboxyethyl)phosphine, an odorless reducing agent more stable and effective than dithiothreitol. *Anal. Biochem.* **1994**, *220*, 5−10.
(69) Levison, M. E.; Josephson, A. S.; Kirschenbaum, D. M. Reduction of biological substances by water-soluble phosphines: gamma-globulin (IgG). *Experientia* **1969**, *25*, 126−127.
(70) Kantner, T.; Alkhawaja, B.; Watts, A. G. In Situ Quenching of Trialkylphosphine Reducing Agents Using Water-Soluble PEG-Azides Improves Maleimide Conjugation to Proteins. *ACS Omega* **2017**, *2*, 5785−5791.
(71) Boeneman, K.; Delehanty, J.-B.; Blanco-Canosa, J.-B.; Susumu, K.; Stewart, M.-H.; Oh, E.; Huston, A.-L.; Dawson, G.; Ingale, S.; Walters, R.; et al. Selecting improved peptidyl motifs for cytosolic delivery of disparate protein and nanoparticle materials. *ACS Nano* **2013**, *7*, 3778−3796.
(72) O'Brien, E. P.; Brooks, B. R.; Thirumalai, D. Effects of pH on proteins: predictions for ensemble and single-molecule pulling experiments. *J. Am. Chem. Soc.* **2012**, *134*, 979−987.

https://doi.org/10.1021/acsanm.4c04586
ACS Appl. Nano Mater. 2024, 7, 24013−24027